Micro-Deformable Mirror: a low cost technology for cryogenic active and adaptive optics

Sebastien Louis Bonicel

Micro-Deformable Mirrors:

A low cost technology for

Cryogenic Active and Adaptive Optics

Sebastien Louis Bonicel

For the Degree of **Masters of Science**

1999

A thesis submitted to the University of Durham

Micro-Deformable Mirror: A low cost technology for Cryogenic Active and Adaptive Optics

Sebastien Louis Bonicel

Submitted for the degree of Masters of Science, 1999

Abstract

Electrostatically operated bi-directional deflecting silicon membranes can be created using bulk micromachining techniques. The 19-channel Micro-Deformable Mirror, potential candidate for space Active and Adaptive Optics, was built by OKO Technologies. The purpose of this project was to test the mirror, constituted from its silicon membrane and its aluminium coated mount, under cryogenic conditions. The mirror was mounted on a self designed three piece structure and several experiments were constructed to characterise the zero point drift, the maximum stroke and the dynamical response of the MDM. The membrane was tested by interferometry and showed stability within 0.34μm of the initial membrane figure (flat within $\frac{\lambda}{13}$, $\lambda = 0.633\mu$m, at room temperature). Space temperatures are down to 35K and the MDM showed great dynamical behaviour at temperatures down to 86K. Adaptive Optics require a frequency response of the order of 1kHz. C++ programs drove the MDM to frequencies of up to 1.66kHz. As it can work under cryogenic conditions and has high frequency response, the MDM leads to great expectations for inexpensive wavefront correction at infrared wavelengths.

Contents

Chapter 1

Introduction

Telescopes are being built bigger and bigger to collect more and more photons to look further into the past of the universe. But even when used most efficiently, these monsters are limited by their location: behind the atmosphere. This great wall introduces distortions into the light coming from the stars and limits the quality of the images; it also increases the noise due to absorption and emission from different layers of the atmosphere. For these reasons optical and infrared telescopes have three important requirements in order to increase their image quality: good seeing (minimal turbulence), minimal pollution of the air (far from cities as the incoming light is scattered by the particles of the air), and low atmospheric water vapour concentration. Even if the second and third conditions are fulfilled, the telescope still does not deliver a diffraction limited image for the atmosphere introduces phase fluctuations into the light beam. Adaptive Optics (AO) has been introduced in order to recreate 'perfect conditions' for observations, close to the diffraction limit. This chapter gives the necessary background to understand both the reasons and the applications of an AO system. Specifically, we will concentrate on the technique and science available for and with deformable mirrors.

1.1 Cryogenic Adaptive Optics: wavefront correction at infrared wavelengths.

Consider a ground based telescope, its mounting being at ambient temperature. In its movements, the telescope bends slightly under the weight of the structure, the engines of the pointing systems and the instruments radiate heat. The ventilation of the dome only keeps the tem-

perature steady. The whole system is at the ambiant temperature of the chosen site , which even at high altitude, only reaches 263K. When the infrared window is the main purpose of the system (in the K-band at 2.2 μm for example) the thermal background due to the warmth of the telescope must be minimized.

We now go into space. Our telescope is the newest of the new generation and the materials used in the structure can resist very low temperatures. There are, however, fluctuations and errors in the shape of the primary and secondary mirrors, perhaps in the lenses of an instrument or there is an error on one member of the structure or even on the mirror itself... The space-based systems are subject to weight constraints. The latest developments show interests for lighter, deployable optical elements, and this leads to high structure flexibility and thus to the need for shape corrections.

In both cases the aberrations can be corrected by means of an Active Optics (ao) system included in the panel of instruments. In order to reduce the heat radiations of a mirrored surface the only way is to cool the instruments down to very low temperatures, in most cases to liquid nitrogen temperature, 77K, or for a telescope in space to 35K and this in order to reach wavelengths down to the H band (1.6 μm). The simple fact of cooling a device down from 263K to 120K leads to a reduction of 30 in the energy power of the body. In other words the background noise is 5.5 times lower.

Troubles arise quickly because it is known how to cool down cameras or spectrographs but not the deformable mirror of the AO system, for various reasons that will be mentioned later when introducing the different families of mirrors.

The purpose of this investigation is to characterise the performance of a new deformable membrane for cryogenic applications. In its project report *The Next Generation Space Telescope* [16], NASA exposed ten key technologies for NGST and highlighted cryogenic actuators and adaptive and active optics as one of them. It has to be noted that the aberrations of HST due to the misalignment of the primary mirror could have been trivialy corrected with such a device. Included into a cold chamber for ground based telescopes, cryogenic Adaptive Optics (AO) would offer benefits at wavelengths longer than 1.6 μm (the benefits start in H band). AO have a bandwidth of $\sim$1kHz, when ao use a bandwidth of $\sim$10Hz. The first system can be used to correct atmospheric fluctuations, when the second system is enough to correct low time dependant aberrations.

For that purpose we will first introduce the different correcting elements used in AO systems, then focus on an introduction to a simple physical model of deformable membranes. In our particular case, we will investigate the properties of a Micro Deformable Mirror that has been subjected to a series of tests in order to outline its characteristics: zero point drift or the fluctuations of the biased membrane; the maximum deformation of the membrane; and finally the dynamical response and the consistency of the frequency response. The results will show that this membrane is suitable to work at various temperatures (down to 115K) with very little fluctuation, which can be corrected by small voltages, hence it can be used in cryogenic instruments and shows outstanding promise for space-based applications.

1.2 Adaptive Optics systems

To reduce the random variations of the atmosphere, Babcock, in the 1950's, suggested the introduction of a device that would take and analyse the incoming beam and induce a stabilisation of the light beams within the telescope itself. Adaptive Optics was born.

An AO system is composed of three key elements: a wavefront sensor (WFS) that measures wavefront errors; a deformable mirror that compensates for the distortions in the wavefront; and a control system that carries out and synchronises the operations. Dynamic Adaptive Optics represent a class of corrective optics where an optical surface is mechanically or electrostatically deformed to approximate some form of a conjugate of either a static optical aberration or time dependent random variations. Wavefront sensing and loop control provide the time dependent analysis and corrections. The incoming wavefront feeds the wavefront sensor (Shack-Hartmann sensor for example). The wavefront disturbance being measured is imaged onto a lenslet array. If each wavefront were perfect, the lenslet would focus light at its own null position. Local slope variations across the wavefront, however, displace the foci from the null positions. This displacement is directly related to the slope error in the wavefront and can be measured with a quadrant detector. The data feeds a computer that will calculate the wavefront phase based on algorithms, and redirect the information to the deformable mirror in real time so that the sightly slower fluctuations can be corrected.
For more details about wavefront sensors and control systems see [22].

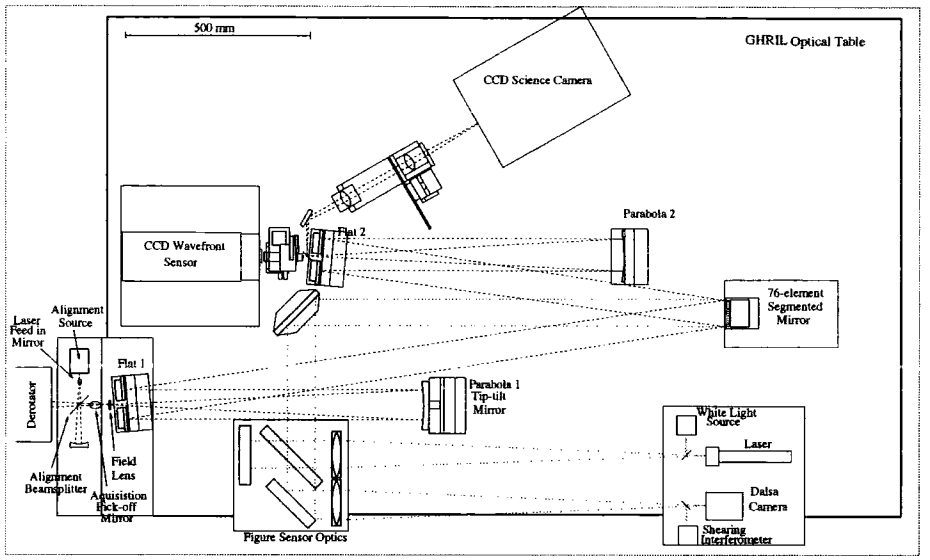

Figure 1.1: Example of an Adaptive Optics System. Schematic of the optical system ELECTRA developed by the Instrumentation Group of Durham University. ELECTRA is an Adaptive Optics system with a 76 segment deformable mirror, a wavefront sensor (80x80 pixel Shack-Hartmann detector), and a series of hardware control devices. In this design, the CCD camera and the Wavefront sensor can be cooled down as they are detectors. The surface mirror is controlled by means of piezo-electric actuators which, even at warm temperatures, have a poor hysteresis response. Cooling down the system would increase this effect. Another problem would be the segments position on the surface and more specifically the contraction of the materials. The instrument would have to be recalibrated often to avoid any light loss by scatered light and misalignement. The solution would be to have the cooled MDM instead of the 76 segments mirror alongside the Shack-Hartmann detector and the CCD camera.

1.2.1 Deformable Mirrors

Wavefront Correctors

General concepts There are two main families of wavefront correctors: inertial and non-inertial [2]. Inertial correctors are those which move a physical mass in order to change the phase of the optical beam. The continuous facesheet and segmented mirrors are in this family. Non-inertial correctors are those which change the phase of the beam through some other process, such as liquid-crystal phase retarders. We mention the segmented mirror family represented by the piston-mirrors and tip-tilt mirrors with their three degrees of freedom (As can be seen in Appendices 5.5.2, piston, tip and tilt are the low order aberrations, first order coefficients of Zernike Polynomials. For those, only 3 degrees of freedom are needed as they occur in single planes and are called 2 dimension aberrations. In order to correct for higher degrees of aberration, 3 dimension aberrations,

several hundreds of degrees of freedom are required. For example, the ELECTRA segmented mirror has 228 degrees of freedom). Deformable mirrors occur in several families: bimorph mirrors, composed of a mirror substrate and piezo-electric electrodes; discrete actuator mirrors, which use a surface divided into segments and a set of discrete force or displacement actuators; 'rubber mirrors' using piezo-electric actuators to mechanically deform the membrane; and finally the membrane mirrors, composed of a thin membrane and electrostatic actuators.

The approach used for wavefront correction is by 'fitting' a membrane to the incident beam as shown in Fig 1.2:

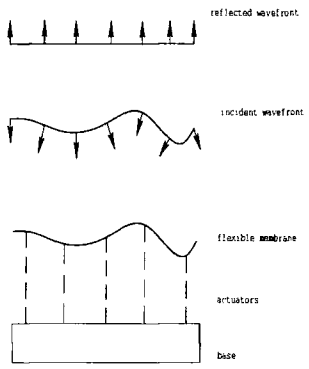

Figure 1.2: Wavefront correction using a flexible membrane. The incident corrupted wavefront is compared to a 'flat' reference and substracted so that half of the phase fluctuations determined by the wavefront sensor can be compensated for (only half of wavefront phase differences due to reflection doubling). This information from the detector feeds the loop control which transfers them and changes the shape of the membrane using the set of actuators. For more information refer to [22].

The incident wavefront is distorted by the random variations of the atmosphere. It arrives and strikes the deformed membrane which ideally would have the exact shape of the wavefront. After reflection on the surface, the pupil wavefront has become 'flat' (phase fluctuations have been compensed for by the difference in optical path of the three dimensional surface) and can be focused on to a detector for analysis.

There are three primary parameters, common to all families, which affect the quality and the adaptibility of a deformable mirror in an AO system: number of actuators; temporal control bandwidth; and the maximum actuator stroke.

For astronomical observations, these parameters are usually a function of the required

Strehl ratio S. [1]

Number of actuators and wavefront variance The most important parameter is the Fried parameter which defines the real image quality at a certain wavelength taking into account the conditions of observations:

$$r_0 \propto (k^{-2} \int_0^\infty C_n^2 dz)^{-\frac{3}{5}} \tag{1.1}$$

k is the wave number, $\lambda/2\pi$, of the incident beam, z is the altitude, C_n^2 is the atmospheric refractive index constant. The number of actuators needed on a specified system is a function of the diameter of the telescope and the actuator spacing

$$N_a \propto (\frac{D}{r_s})^2 \tag{1.2}$$

From that we can see that the number of actuators is a function of the telescope one uses. The wavefront phase errors to be corrected link the two previous parameters, r_0 and r_s, and shows the importance of the atmospheric refractive index structure constant C_n^2

$$\sigma^2 \propto (\frac{r_s}{r_0})^{\frac{5}{3}} \tag{1.3}$$

The value of C_n^2 is determined experimentally. One way is to measure the temperature structure constant C_T^2 (Appendices 5.5.2) and then calculate the constant at every altitude. C_n^2 describes the strength of the turbulence at a given altitude. Well defined turbulence statistics are only weighted by this parameter. For more information on the atmospheric constant refer to the introduction on the theory of atmospheric turbulence (Appendices 5.5) and to [10],[11] and [13].

Maximum stroke and frequency response The stroke required for the mirror is determined by the range of wavefront phase errors. For AO, the phase (in particular for the first optical aberations) can be approximated and has been introduced in Equation 1.3. As the maximum stroke is a function of C_n^2 and D, the required frequency response is function of the strength and speed of a turbulence at a given altitude. For a given turbu-

[1] S being the measure of imaging performance. It is the ratio of on-axis intensity of an aberrated image to on-axis intensity of the unaberrated image (diffraction limited image).

lence state, this is the wind velocity in the considered cell that determines the required frequency response of the mirror [19], it is called the Greenwood frequency:

$$f = \frac{0.4v}{\sqrt{\lambda L}} \tag{1.4}$$

where v is the mean wind velocity in the turbulent layer, λ is the wavelength of the incident beam and L is the average thickness of the turbulent layer.

The main hypothesis behind the theory of this frequency is that at a given altitude one considers frozen turbulence, where the eddy velocities are neglected, and the turbulence state is considered as static as the atmospheric shell is carried across the observing path by the wind of velocity v.

For example, if one considers a moderate turbulence and works in the near-infrared light ($\lambda = 1.0\mu$m) with a 1m diameter primary mirror and a Strehl ratio of 0.2, a deformable mirror would require 400 actuators, a bandwidth of 20Hz and a stroke of 2 μm. The timescale for the variations in the distortion is in the order of a few milliseconds in the optical. This means that a close-loop control bandwidth of 1kHz is required, as an upper limit. To achieve a control at 1kHz, the natural frequency of an actuator should be around 10kHz.

Considering a circular membrane and the fact that the tension on it is function of the constants E, σ and ν [6] the natural frequency of an actuator is given by:

$$f_n = \frac{10.21h}{2\pi d^2}\sqrt{\frac{E}{12\sigma(1-\nu^2)}} \tag{1.5}$$

where h is the membrane thickness, d is the spacewidth between the actuators and the membrane, σ is the density of silicon, E is the Young's modulus of the membrane substrate and ν is the Poisson's ratio[2] of the membrane. The development of the model of a membrane mirror is given in Section 3.2.1

[2]The Poisson ratio is the ratio of the absolute value of the strain in the lateral direction to the strain in the axial direction of the solid under load.

Comparing mirror technologies

Although the choice of one of these technologies has much to do with cost, frequency response, size etc., there are advantages and disadvantages when choosing one or the other. For example a piston corrector scatters light from the sharp edges of the segments but to achieve a good optical quality these segments would have to be sharp. When using a coronograph, for example to detect planets around bright stars, this scattered light would corrupt the image quality and might be unacceptable. Kitchin (1991) discusses the compromises that are necessary with these devices [3]. Membrane mirrors have recently been at the forefront of the development of adaptive optics because of their size and specifically because they allow the reduction of the size of the instruments. The increasing number of instruments at the focus of the telescopes has lead optical designers to consider that they now have to reduce the size of the individual devices, cameras, spectrometers, AO etc. as much as possible.

Because current implementations of adaptive optics are very expensive, the great challenge would be to reduce both the cost and the size of the device. We are going to show that the Micro Deformable Mirror is an inexpensive and efficient device for both ground based and space telescopes and with its 15-25mm diameter it will considerably reduce the amount of space wasted. We will also demonstrate that it can work at 115K, with good reason to believe it will work colder.

1.3 The Micro Deformable Mirror

OKO Technologies, specialists in the fabrication of micromachined mirrors, have created and developed a series of silicon micromachined devices (Fig. 1.3). These micro-opto-electro-mechanical systems (MOEMS) have recently emerged to serve the increasing demand for low-cost technology. They provide miniaturised, reliable and precise control of a continuous surface. The small electrostatic actuators mixed with a silicon membrane offers all the characteristics expected of a wavefront corrector.

1.3.1 Silicon technology

Because silicon can be a conductor, a semiconductor or even an insulator, it presents all the necessary characteristics required to build small, cheap and reliable components. The art of

silicon now allows a mixture of electronics devices with micro-mechanical and micro-optical sensors which simplifies and increases the number of applications. These components have low inertia, and can be positioned accurately with small forces, even at high frequencies. IC Technology, from silicon micro-machined shutters and thin deformable membrane mirrors (used as light valves in computer memories) to thermopiles, is now available and promises a great future[1][6].

1.3.2 Description of the device

The subject of this report is the 19 channel Adaptive Optics System Micro Deformable Mirror (MDM). It has been fabricated at OKO Technologies using the technology of silicon bulk micromachining.

Bulk-Micromachining is the process of fabricating mechanical structures by etching the bulk of a wafer and more specifically by the use of all three space directions. Normally and it is our case, silicon is the basic substrate material. The technological control of the material is essential for the sensitivity and miniaturization of a device. Two basic methods are used, wet chemical etching and dry etching. The MDM is a product of wet chemical etching using KOH as an anisotropic etchant. Considering that the etch rate is much higher in the $< 100 >$ that in the $< 111 >$ direction of the crystal[3] and assuming that the etch speed is well understood and the time controlled, it is possible to create mechanical structures.

The device is separated into two main bodies (Fig 1.4):

The chip It contains a circular silicon nitride membrane coated with aluminium in order to create a high-reflective film to form the mirror. Silicon nitride is a good insulator, so the Al layer can be used as a capacitor plate for the electrostatic control of the membrane shape. Because the $< 100 >$ and $< 111 >$ crystallographical planes are etched at different speeds the final shape of the etched chip is always rectangular. Using a special etch mask, it is however possible to create approximately circular membranes. In terms of geometry the actual membrane of the MDM is not perfectly circular, but the deviation from the circular contour being less than 0.2mm which is acceptable for the developments

[3]Three dimensional crystaline structures are usually visualised more easily by a set of plans cutting the lattice in parallel sections. The position of these sections is determined by the value of the Miller indices (h,k,l) which are functions of the three dimensions of the crystal cell. In our case, the plan $< 111 >$ is the plan cutting the unit cell on its biggest diagonal.

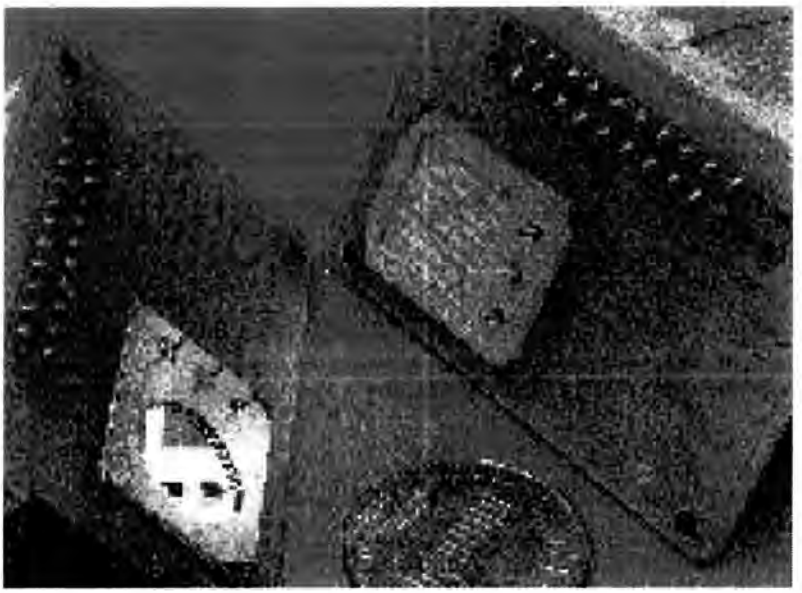

Figure 1.3: Picture of the device. The approximately circular membrane has a diameter of 10mm. Fig 1.3 shows the two sides of the MDM with on the bottom left corner of the membrane on the glass wafer resting on the PCB board. The input voltage connections can be seen at the top of the PCB board.

of models, the membrane will be assumed to be perfectly circular [4]. The experiments have shown that the boundaries of the membrane can be defined so that the membrane is perfectly circular. As the tests run were measuring the fluctuations of the flatness of the membrane, only a central part of it was taken into account using a circular mask during the interferometric measurements. It is important to note that the edges of the membrane were not completly symmetric so that the tension on the membrane was not symmetric and a slight natural astigmatism was present. We however made the assumption that the membrane was circular.

The PCB support The 19 electrostatic pads (also called the 19 channels in relation to the addresses of the controls within the software provided with the mirror which will be introduced later) are electrodes controlled via a bias voltage V_b and a structure of controlled voltages $V_1 ... V_n$. This bias voltage is important as it will be shown that in order for the membrane to work effectively at low temperatures it has to be biased. The value of the bias is determined by the *working range* which will be introduced later(Section 3.4.2). The membrane surface is shaped by applying a reference voltage to the Si chip, V_b, and by applying voltages to each one of the electrodes. The spacer makes sure that the membrane does not touch the pads so that the membrane can assume any shape and

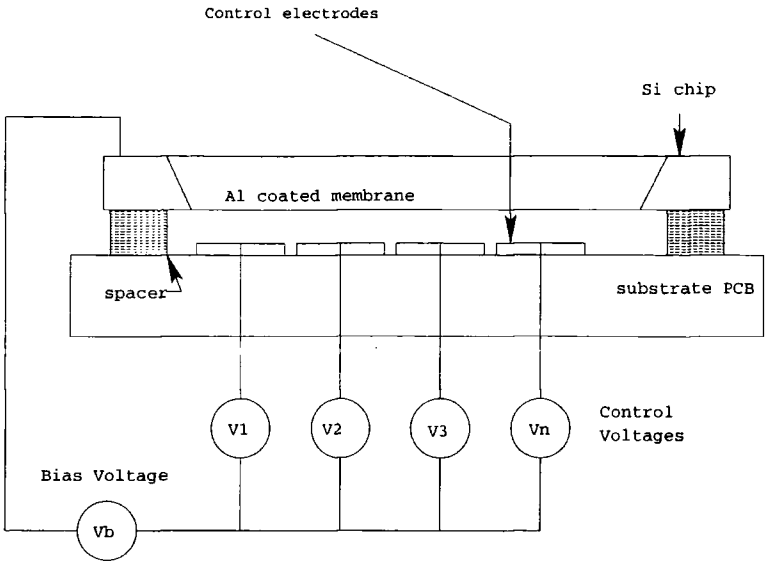

Figure 1.4: Schematic section of the MDM. The input voltage connections of Fig 1.3 make the connections between the control electrodes and the control voltage. The glass wafer supports the membrane and rests on the substrate PCB.

in the worst situation avoid a catastrophic and definitive failure [4]. However, as the membrane becomes a capacitor with the layer of aluminium (non-conducting material) and it is connected to the earth through the wiring there is no chance of a short circuit in a correctly fabricated device.

Table 1.1 gives the technical data of the mirror. These data have been determined by OKO Technologies and serve as a reference for the present research. Certain values like the Initial P-V deviation from plane, specific to each membrane, will be measured, improved and new results will be exposed on this document.

As an optical device, the circular membrane is subject, more or less strongly, to all known aberrations. The major natural defect is astigmatism and the mirror therefore has poor off-axis performance. The distance between the membrane and the actuators is not equal across the chip. The larger deformation at the centre leads to a strong spherical aberration. As we will also see later the mirror can be used as a defocus corrector. Defocus is more than a simple aberration to be corrected, it is one of the criteria that makes a good AO device. The defocus will then be measured at different temperatures as a reference for the surface quality [1].

parameter	value (36 channels)	value (19 channels)
Aperture shape	circular	same
Number of electrodes	36	19
Bias Voltage V_b	0...150V	0...80V
ControlVoltage V_c	0...220V	0...143V
Initial P-V deviation from plane	less than 0.8μm	less than 0.5μm
Main initial aberration	astigmatism	same
Frequency range	0...100Hz	0...12kHz
Max. deflection of the mirror centre	7 μm	4.5 μm
Maximum optical load	0.03W/mm^2 for λ=1.06μm CW	no data
Surface defects	up to 20 dust particles, up to 2 coating defects with area of 1mm^2 each,total scattering less than 2%	no data

Table 1.1: Technical data of the MDM

1.3.3 Actuator structure

The membrane of the MDM is mounted over a set of 19 electrostatic electrodes in copper. The structure of the PCB plate is given in Fig 1.5. The electrode structure is directly patterned on the metallisation of the PCB.

The mirror shape is controlled by two high-voltage amplifier boards supplied by OKO Technologies. Each board contains 20 non-inverting DC amplifiers. Each amplifier has a gain of 53, which permits a range of variations on the voltage of 264V maximum (with 0-5V inputs). The value of the voltage can be increased or decreased by means of localisation of the address of the output considered on the electrodes network.

1.3.4 Advantages of the MDM

The advantages of the MDM are numerous. First of all the cost of such a device is considerably reduced ($2000 per actuator for the ELECTRA mirror against $100 for the MDM) despite the high technology put into the silicon membrane.

Size of the device A desirable attribute of a deformable mirror is that it should be designed so that its main compononents are in modular form: small and easy to replace. This will simplify the assembly of the entire system and reduce the load and weight put on the structure of the host. The first advantage then is the reduction of the size of the device

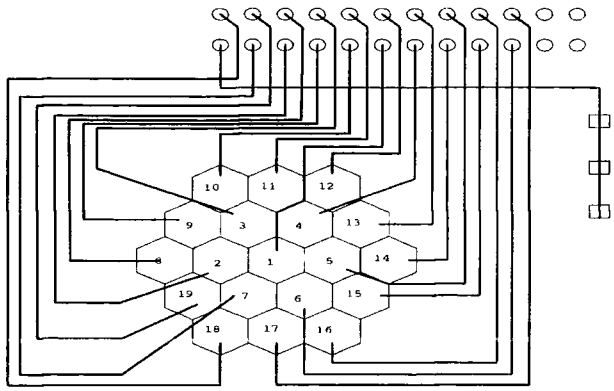

Figure 1.5: Actuator structure fabricated using PC board technology. The 19 electrodes are made of copper and copper wires make contact between the actuators and the voltage pin-input. The first pin is connected to the membrane and to the ground.

while keeping every characteristic necessary for a good mirror. For the 19 channel MDM, the circular membrane is 10mm in diameter and the whole mount, including the printed board, reaches 30x30mm^2. As a comparison, the ELECTRA mirror introduced earlier (Fig 1.1) had 76 segments and a diameter of 76.2mm; a 76-channel MDM would have a diameter of 20mm. Because cost scales with cold volume, the MDM could reduce the total cost of a cryogenic system.

Frequency response The second point is the frequency range, from 0 to 100Hz, or higher. This characteristic will be tested and analysed (Section 3.5), but the response of the mirror should be very fast and it could reach frequencies up to 1.3kHz [1].

Optical quality The design tolerances are achieved with submicron precision. On one silicon wafer used to create the membranes, one can fabricate 16 membranes where at least one will have an optical quality of about $\lambda/10$ [1]. The residual mean square (rms) from the plane is estimated to be around 0.077μm or $\lambda/8$ for the HeNe laser ($\lambda = 0.633\mu m$) used in the interferometric studies of the surface [1].

Continuous optical surface: Some mirrors are composed of an array of small mirrors where each one is activated by its own actuator. The silicon membrane of the MDM is continuous, with no edges, bleeding, scattered light or absorption from the joints.

Electronics Since the array of electrodes is controlled by a simple PC, the mirror's electronics are relatively simple. The input and output are electrical data. This simplifies the tasks

of the main control and greatly reduces hysteresis problems

1.3.5 Drawbacks.

However, such a small device has several drawbacks which, although they are mentioned here,do not limit the quality of the MDM .

Non replaceable and different actuators The electrodes can be considered as highly accurate and reliable under stress. But it is impossible to replace one actuator without disturbing the entire mirror. The whole structure would have to be changed . The mirror would also need to be recalibrated. The solution is to put the system of electrodes under a nominal voltage off condition. But even then the non-linearity of the actuator X will differ from the non-linearity of the actuator Y. The simplest way to repair a mirror would then be to replace it which makes it easy in case a problem arise but which inevitably leads to the re-calibration of the AO system.

Tension The tension on the membrane is high. Although the silicon chip is made very carefully, a membrane larger than 10 mm is fragile. Low-stress high-quality membranes have been developed with a thickness of up to 10μm and with the addition of a nitride layer. The conditions of handling and moving the mirror make the experiments slower (we ought to mention that further research should be done on this matter to determine whether the membrane would support launch accelerations or any strong shakes). This is another consequence of the high tension on the membrane. No dust should penetrate the air gap between the electrodes and the chip otherwise they would puncture the very sensitive membrane. The first steps of our experiments were on a 'bad' mirror which was marked to have some dust between the membrane and the actuators.During an experiment the membrane broke. After few experiments we got to the conclusion that dust might has been the cause of the destruction of our 'bad' mirror as a voltage was applied, the dust could have touched the membrane and punctured it. The conclusion is that no dust should penetrate the air gap previously defined.

Uniformity The model of circular aperture needs (see the detail in the next section) the assumption of uniformity of the pressure over the membrane. When the deformations

of the membrane are comparable to the thickness of the air gap, the deviations from a parabolic response can be quite large.

Low order correction A very significant disadvantage is the fact that the MDM can only correct low order aberrations (up to spherical) due to the restricted number of actuators (which can be solved by using a bigger MDM. We have, for that purpose, a 37-channel mirror). The corrections are, however, sufficient with the low orders to improve the image quality by a factor of 70% as can be seen in Appendices 5.5 Table 5.3.

1.3.6 Conclusions

The 19-channel Micro-Deformable Mirror, built by OKO Technologies, represents a good candidate for Cryogenic Adaptive Optics for its size, its complex but reliable technology, its array of actuators easy to control, its cost... We have seen that it has several minor drawbacks such as its capability of correcting only for low order aberrations. The following chapters develop several experiments that have been run to complete the understanding of the characteristics of the membrane and its stability under evolving thermal conditions.

Chapter 2

Requirements and setup of the experiment

2.1 Introduction

The concept of cooling down an entire AO system is not new, but its applications have been put aside for several reasons. First, the technology of the flexible mirrors did not allow such drastic environmental changes: the properties of many of the materials that are commonly used change at low temperatures and become difficult to control in terms of shape and frequency response. Examples are numerous: piezo-electric actuators having problems of hysteresis at low temperatures; bimorphs mirrors would not resist a cooling as the two layers would contract differently and deform the surface; segmented mirrors have edges alignment problems; liquid crystals would simply freeze. Second, and this is one of the numerous advantages of the MDM, other devices are often too big to meet the space restrictions of a cryogenic dewar alongside other instruments. This chapter introduces the concept of low-temperature techniques applied to the Micro Deformable Mirror. We will look at the requirements of the whole system and introduce the important parts of the experiment.

2.2 Low-temperature techniques

The low-temperature technique to be adopted depends partly on the required temperature, thus of the refrigerant. There are two main groups of techniques (e.g see [14][15]). The first

is characterised by mechanical expansion or contraction techniques that require the change in volume of an isolated piston (by expansion with the Joules-Thompson Expansion or by External work with the Claudes-Liquefier, for example). The second is entirely based upon the use of refrigerants. Our experiment is in the second group. We needed a considerable temperature range and liquid nitrogen was the best candidate as it is the cheapest refrigerant, easy to manipulate and relatively easy to control. It is beyond the scope of this report to describe all the low-temperature techniques. However, it is important to introduce the key device of a cold experiment: the cryostat.

2.2.1 Cryostat

The simplest technique was to use a commercially available liquid nitrogen cryostat. It provided a light, cheap, and relatively efficient way of cooling down a small device like the MDM. The dewar we used was the Oxford Instruments 2l bottle dewar described in Appendices 5.4.2 (Fig 5.11). It responded to all the requirements of the experiment.

Size The whole system is 240x377mm and does not weigh more than 5Kg empty. It makes it easy to carry.

Bottle The dewar contains a 2l bottle with walls of aluminium (one of the best thermal conductors, alongside copper). The refrigerant is then contained in the bottle which is situated inside a second stainless steel double-walled bottle, thermally insulating it. The air between the refrigerant bottle and the outer walls is evacuated.

Temperature range The inner tank is isolated from the outside. The temperature limit expected when using liquid nitrogen is 77K. In theory the cryostat can then operate at any temperature between 290K and 77K. We will see, however, that this limit is slightly higher due to heat exchanges with the surroundings. Some improvements have been made in order to minimise these exchanges.

2.2.2 Heat exchanges

The energy flow inside the dewar was subject to three processes: convection in the gap between the walls, conduction through the walls and the wires and most important of all radiations from the $\sim 2\%$ black body constituted of these mirrored walls. The heat loss were mainly due

to the last one as vaccum is produced inside and thus limited conduction and convection. Using Stefan-Boltzmann relation and thermal equilibrium relations

$$\Delta E = \sigma \Delta T \tag{2.1}$$

where σ is the Stefan-Boltzmann constant,

it was found that the heat loss of the dewar by radiative effects did not reach 0.2mW. Other concerns were the connections through cryogenic wires (wires with an insulated core that resist cryogenic temperatures) that made a link between the membrane and the outside. A quick calculation using the simplified equation of heat flux through solid media

$$q = hA\Delta T \tag{2.2}$$

where A is the average section of the wires and H the heat transfer coefficient (W/cm^2), has shown that the amount of energy lost by conduction through the cryogenic wires was less than 2mW /wire. However, 30 of them were connected to the outside and played a significant part in the process and appeared to be the main source of heat loss. The fill/exhaust port in the back of the dewar stayed in constant contact with the warm room which lead to LN_2 loss by convection. However these loss were minimal and usually neglected. The vacuum state of the air gap lead to a relatively good and more stable thermal equilibrium where the cold bottle was in physical contact with the mirror (see next section). It has to be noted that the dewar has a specific time of thermal stability (see Appendices 5.4.2, Fig 5.12). We put the emphasis on the heat loss because they represented a problem in terms of stability of temperature at the surface of the MDM. They were however very small and as can be seen in Appendices 5.4 Fig 5.10 the dewar stays very stable for more than 20h.

2.2.3 Thermal expansion

When the temperature of a solid changes a corresponding change in volume V takes place. Most of the materials we use are homogeneous in their expansion, they then have a symmetry in their response to a thermal stress. If a typical dimension of the solid is l_0 then one defines the coefficient of linear thermal expansion α by Equation 2.3. α is usually taken as a constant,

then for a constant stress process

$$\frac{l - l_0}{l_0} = \alpha \Delta T \tag{2.3}$$

where l_0 is the one-dimensional length of the solid at T_0. Stainless steel and aluminium have relatively low thermal expansion coefficients which make them fairly reliable when working at cold temperatures. These coefficients are very close, and even though they are function of the temperature, they stay in the same order of magnitude. This is not the case for the MDM where, as we will see later, this is the main problem: reducing the thermal expansion of the mount and the mirror holder. It needs to be emphasized that the mirror itself is very stable thermally. The problem occurs when it is attached to the dewar by an external, designed piece inducing thermal and mechanical stress on the structure.

2.3 Design of the L-bracket

Considering all the characteristics that make a good dewar, we had to find a way of installing the mirror inside the system without disturbing the thermal equilibrium and with minimal heat loss. The thermal expansion and the heat exchanges had to be taken into account in order to optimize the efficiency of the cryostat. The design of the different parts are given in Appendices 5.1. The purpose of this section is to explain the different characteristics of these components.

2.3.1 Design

The mechanical design of the components has been a big part of the research and constitutes a key point for further studies on the MDM.

warm temperatures The first idea was to fix the mirror on an aluminium L-bracket and test it at warm temperatures. This series of experiments did not require any important calculations in terms of contraction of materials but it was fundamental to start understanding the heat process on the membrane and thus to design a component that would suit the future steps. Following that idea, we designed the aluminium L-bracket to support the MDM (Appendices 5.1.1).

low temperatures The next step was to fix the MDM inside the dewar. At first, the MDM was mounted only on the L-bracket and diodes and resistors glued on to the glass wafer

that supported the membrane. But the surface of the wafer did not resist the thermal amplitude of the experiments and its thin aluminium coating broke under thermal stress. We had to find another way of making a thermal contact between the temperature sensors and the membrane.

This problem leads us to consider a three piece mount that would cover the membrane without touching it and by means of an indium gasket would make a thermal contact. Appendices 5.1.2 gives the details of the three independant parts (pictures of them are in Appendices 5.1.2 Fig 5.5 and Fig 5.6). A lower plate (Fig 5.4) supported the whole mount and was fixed to the L-bracket. The MDM was then accurately fixed to it at only two points (two far corners of the PCB board). On top, the middle plate (Fig 5.3) made the basis to receive the top plate (Fig 5.2) on which the components were glued. The middle and bottom plates were fixed using screws (with vacuum holes to avoid any air trapped in the holes). The top and middle plates were fixed using light springs to allow a certain contraction without putting to much stress on the middle plate.

The top and lower plates were made of aluminium for its density and its high thermal conduction. The membrane was then connected to the cold plate of the dewar. The middle plate was thermally non conductive in G-10 to isolate the mirror's surface. This was necessary to allow mirror temperatures different to 77K..

2.3.2 Materials

Aluminium Aluminium is an appropriate material for our purposes. It is brittle, has a good thermal conductivity, has a low density and is easy to machine. The balance between its cost and physical properties makes it a very good material for low temperature components, and in our case for a LN_2 mechanical components.

Silicon We have introduced silicon as a semiconductor (Section 1.3.1), but it is a key design aspect of the MDM. Its thermal conductivity is very high but it is also the only available material that can be used.

Table 2.1 gives the values of the important features of these two materials.

The values of this table have been found in [14]. The thermal conductivity of any substance, gas, liquid or solid, is not constant and depends on the temperature. However, in

Table 2.1: Characteristics of important materials used in the industry.

Materials	Al. Alloy(6061-T6)	Silicon
Ultimate stress(MPa)	310	
Young modulus(MPa)	70000	110000
Density(Kg/m^3)	2800	2330
coef. of thermal expansion(K^{-1})	23	2.5
Thermal conductivity(W/m.K)	4	835

the temperature range considered (77K-290K), we will assume them constant.

Silicon has a very low thermal expansion coefficient. As a result, the membrane is very stable at cold temperatures. Therefore, the problems will come not from the dewar body changes but from the aluminium parts of both the MDM and the L-bracket.

2.4 Experiment

This section details the experimental setup. It provides a general layout and some explanations on the use of the main physical parts (computing facilities and voltage control, connections) of the whole system and more specifically details the process of data acquisition using the *Zymod* inteferometer alongside its data acquisition software *Zymod*.

2.4.1 Setup

The laboratory optical setup is shown in Fig 2.1. Each one of the individual parts is numbered with a letter and described first how it is connected and how it interacts with the rest of the system and then individually.

The two main parts of the experimental setup are shown in Fig 2.1. The controller centralises the data from the interferometer and distributes it to the video monitor, the video digitizer and the PZT interface. On the other independent subsystem, the main PC runs a series of programs that control the output voltage (for a complete description of the programs see the next chapter). The output voltage of channel N[0...19] (or 36 depending or whether one or two of the digital boards are connected) of the 8-bit 19-channel DAC board(s) is controlled

by sending integer (a factor of 5V) values V[0...255V] to the output port BA+N (BA=Base Address). The two amplifier boards, fed by the power supplies, limit the voltage that reaches the electrodes. A ribboncable connects the amplifiers to the military connector on the socket of the dewar and links the channels to the electrodes. The control loop is then closed.

The MDM is inside the dewar and a laser illuminates the surface. The light reflected from the surface of the MDM interferes with the reference beam and the fringe pattern feeds the interferometer which transfers the data to the *Zymod PC*. The shape of the MDM can be changed by setting the voltages on the grid of electrodes controlled by the PC in ***F***. This PC is connected to two amplifier boards in ***H*** each of which has a gain of 53.

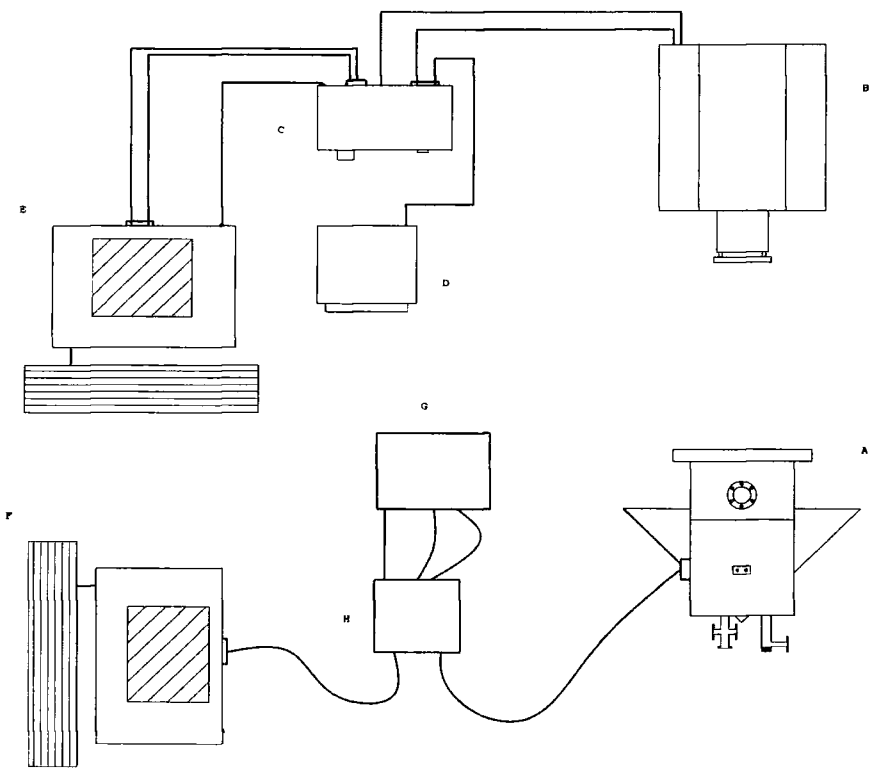

Figure 2.1: Optical setup of the experiment. The components letters are detailed in the text. The Adaptive Optics System consisted of the MDM itself in the cryostat ***A***, power supplies ***G***, amplifiers boards ***H*** and the MDM control electronics ***F***.

The output voltage from the amplifiers goes to the MDM via a military connector on ***A***(there is no exposed voltage on the whole system).

On the other part of the experiment, the *Zygo* (***B***) grabs the interference frames and sends them to the controller unit ***C*** which is connected to both a video monitor ***D*** and the main *ZyMod* PC ***E*** running the *ZyMod/PC* software.

The MDM is located inside the dewar **A** and cooled down with liquid nitrogen. The cryostat is a product of Oxford Instruments-Research Instruments. It provides both a small volume, is easy to carry and have a high stability cold plate. It is mounted on a 5 axis (3 orthogonal translations and 2 tilts) mounting stage. The mounting stage is part of the Zygo unit composed of the Zygo Production Test Interferometer (PTI) in **B**, a surface characterisation system which delivers a dual aperture-33mm and 102mm diameter HeNe laser beam using a three mode transmission element. It has the advantage of being well collimated and very stable. The PTI with the video monitor gives a testing accuracy of $\lambda/20$ which is the order of magnitude of the theoretical flatness of the MDM. The *Zymod* Controller unit **C** contains an amplifier to drive the *Zymod* Phase Shifting Adapter from signals derived from the controller interface board. It also provides video gain adjustment. A 300mm diagonal video monitor with a 700 lines resolution allows a visual appraisal of the interferometric tests **D**. The final part of the Zygo unit is the *Zymod* PC in **E**. It is the main controller which runs the *ZyMOD/PC* software. It contains the video digitizer board and the PZT interface. See section 2.4.3 for details of the data acquisition process.

The MDM control PC **F** controls the voltages applied to the MDM. It contains two digital boards (two boards are required in the case of the 37-channel MDM. In our case only 19 channels were controlled which only required one board). The output voltage is set by sending integer values V[0...140] to the output port of the digital board which converts the digital signal into an electric signal sent to the amplifiers and then to the membrane. Several programs in C++ have been written under the Symantec project environment in order to control the shape of the mirror under different conditions, at different frequencies. They will be discussed in Section 3.5. The signal is sent from the MDM control PC to the amplifier boards with +15V, -15V and high voltage power supplies **G** producing a maximum voltage of 250V in theory. For the safety of the membrane the maximum voltage applied was 140V, which was sufficient to test the mirror. Each amplifier board (**H**) contains 20 non-inverting DC amplifiers for which each has a gain of 53. Each amplifier was connected to one actuator and provided an output voltage of 1 to 140V (with a 1 to 5V input from the control PC via the digital boards). Only 19 of them are connected to the mirror as the membrane was grounded and represented the 20th channel. It was recommended ([4]) to connect it to the 20th amplifier to bias the mirror.

2.4.2 MDM inside the dewar

The MDM has been mounted on an L-bracket fixed on the cold plate of the liquid nitrogen bottle. The thermal contact is good as the bracket is in aluminium. Here, we have to divide the thermal system in two: the cold plate with the L-bracket(Aluminium) and the MDM with its mount(PCB board—Glass mount—silicon-nitride membrane). The distinction is important as the materials used in both parts are very different and thus thermally incompatible. We used a thick copper wire fixed on the top plate (Appendices 5.1.2 Fig 5.2) which makes contact between the cold plate and the surface via an indium gasket. The inner dewar air would then be pumped out which eliminates part of the effect of heat flow by convection. The majority of flow from the cold plate goes then to the very thermally conductive mirror mount.

Figure 2.2: View of the inside of the dewar, the whole system L-bracket—MDM being on the cold plate. At the centre, the connector (left) makes contact between the outside and the L-bracket; the membrane is mounted on a PCB board resting on the middle plate (Appendices 5.1.2 Fig 5.3) and on top of the PCB board, one can see the top plate (Appendices 5.1.2 Fig 5.2) on which are glued diodes and resistors for temperature control.

2.4.3 Interferograms

The *ZyMOD/PC* software, working under DOS environment, is a powerful data aquisition tool. The fringes in an interferogram are located by sets of three coordinates, x and y as the fringe center coordinates of the input image and m the fringe order number. The interferometer grabs pupil images by scanning the entire grid of this pupil and entering the values of intensity or

phase of each point into an array which is then transmitted to the software. A phase value is assigned to a point of the grid in function of the reference determined by a phase shifting algorithm that calculates and compares the relative values of multiple phase-shifted digitized interferograms. Linked to the transducer of the *Zymod PC*, the reference is the reference mirror of the interferometer. The plane of the interference pattern is then scanned one knot at a time and stored at a pre-selected ramping speed and signal to noise ratio. Each one of the points is independent. This leads to a uniform sampling grid. Fig 2.3 shows examples of interferograms. The configuration of the scanner was chosen so that:

-the data acquisition was as slow as possible to average out the laser fluctuations (ramping speed of 8. The scale being 1 for the fastest and 8 the slowest). The laser fluctuations are due to the thermal variations of the laser cavity when it is switched on.

-No smoothed intensity as it tended to miss some bad pixels. The reason for the loss of data is that when the convolving 3 by 3 cell option (smooth intensity) is used, it can lead to phase errors where the regions of valid pixels are compared to regions of invalid pixels. It is particularly the case with the pupil edges and more specifically in the case of a deformed surface (if the membrane is under high voltage creating abrupt and unresolved regions for example).

-The noise threshold at the minimum (1), where the scale (from 1 to 255) represents the range of digitized intensity values, again to avoid loosing bad pixels which would be under the threshold. By setting the noise at the minimum, we ensure that the interferogram is well resolved and even a bad pixel would appear, on a low scale, an average of its neighbours.

-and finally, the area was as small as possible to reduce the time of data acquisition and we were able to reduce the effects of the pupil edges by sampling a slightly smaller area.

In order to reach a high spatial resolution of the pupil plane (thus the membrane image), the interference pattern was limited to a single fringe (by selecting an area of the pupil, using a mask provided by the software, which gave us a reliable set of data). After some tests, a balance between the speed of data acquisition (not too slow to avoid any air variations in the optical path or any vibrations), the signal to noise ratio of the measurements, and the resolution was found which produced very detailed phase and intensity maps.

The software features several corrections on the measurements. First we have seen that the surface to be analysed is divided into a grid of points localised by three coordinates (x,y,m). As any of these points has an optical phase measurement, even on the edge of the pupil, there are no mapping distortions of the wavefront and the test surface. The sampling of the wavefront is uniform and occurs over all the points. As a result, the phase measurements are independant of intensity variations across the pupil. Second, the points within the selected area are modulated, due to the fringe modulation of the interference pattern, which differentiates them from the points from outside the pupil that do not vary from the average intensity during the modulation period.

2.5 Conclusions

The design of the components holding the MDM inside the dewar was critical and the whole device appeared to be working reasonably well. The system including the dewar and the MDM was small and easy to carry or to modify. We noticed however a major drawback on the introduction of the cold plate: the thermal contact between the top plate and the membrane induced a noticable mechanical effect which distorted the membrane mount. Further work should be done in order to improve the mechanical contact on the membrane which already suffers from astigmatism.

The different tools used for the experiments were accurate enough to rely on the data provided by the interferometric studies (Fig 2.3) and start quantifying the important key points of a good deformable mirror.

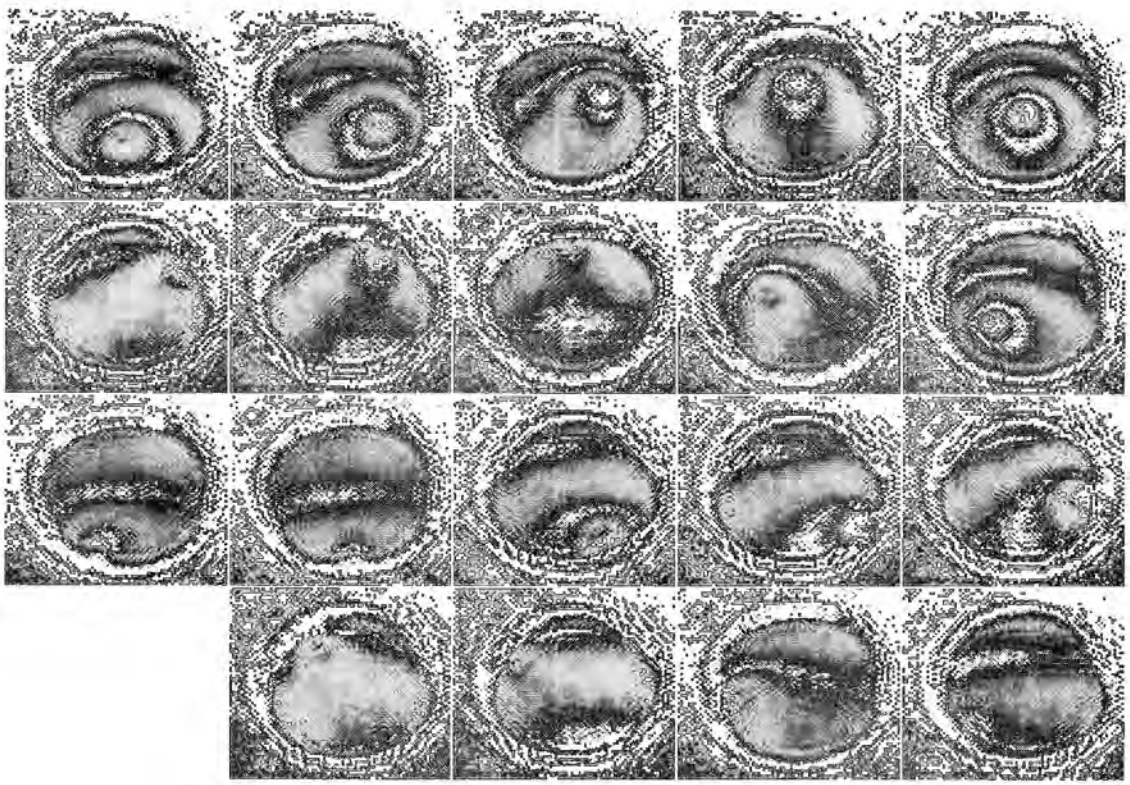

Figure 2.3: Interferograms of the influence functions of the 19-channel mirror. Each actuator was set to a voltage and the pattern of the surface recorded. The data area has been selected such that the data acquisition process was limited to the effective area of the mirror, the area containing the peak of the influence function. The software removes the pupil edges and the effects of diffraction. Only the flat surface is missing from this picture.

Chapter 3

Results

3.1 Introduction

In order to test the MDM effectively, three series of tests were run. The zero point drift of the membrane was the first, in other words how the membrane tension varies if no external load (voltage) is applied, or with a constant bias. It is a fundamental characteristic of any AO mirror. The behaviour of the 'flat' membrane under fluctuating temperatures is critical as the mirror will have to be calibrated and any surface variations would falsify the results. It is then important to quantify these variations or in the best case to verify the perfect thermal stability of the membrane. The second test was the response of the membrane versus the temperature and the maximum stroke reached, which, as we have seen in Chap.1 Sect.1.2.1, is a key point of a deformable mirror. How will the maximum stroke be affected by the drop in temperatures and will it still be enough to correct big aberrations if it decreases with temperatures? The final test was the dynamical response of the membrane in order to verify the constancy of the frequency response at different temperatures. An important feature of the MDM to know is whether or not the membrane can support medium to high frequencies at low temperatures in the first place and in the end to actually quantify the variations at these frequencies as a function of temperature.

In this chapter, we give the procedures followed and the results of these experiments.

3.2 Warm temperature results

Some work has been done by Gleb Vdovin et al. [21] and very recently by Dainty et al. from the Imperial College in London (results exposed at the Durham UK Adaptive Optics Conference, 21st May 1998). The main purpose was to develop a model and to test it dynamically on the membrane. We will see that our results fully confirm the work that has been done and that these conclusions concerning the optical quality, the frequency response, the dynamic response of the membrane are unaltered at cryogenic temperatures. Thus, MDMs show outstanding promise for cryogenic and space-based AO.

3.2.1 Membrane model

In 1903, Prandtl (see Tyson [22] and Saada [7]) developed the analogy between the differential equation of a stretched elastic membrane initially flat and the differential equation of such a membrane blown up by air pressure from the bottom. In our case this stress applied on the surface is the voltage difference between the membrane and the bias electrodes inducing an electrostatic pressure P, and then a tension T causing the deflection along the z-axis.
The mechanical model we expose here is simplified in a way that only a few notions from the theory of elasticity are needed in order to find a balance between Prandtl's simplistic model and modern development of thin membranes [6]. Some assumptions must be made in order to satisfy the model:

- The thickness of the membrane does not reach 5μm which leads to the diameter to thickness ratio being very small. For that reason its stiffness D can be neglected [6].
- The mass per unit area of the membrane is constant.
- The membrane is completely flexible and the lateral tension due to the hard boundaries keeps the shape, circular for our purpose. As we have neglected the stiffness of the thin surface, it naturally follows that the membrane is free to bend and offers no resistance.
- The boundaries of the membrane are not free.
- The deflection of the membrane S(x,y) is small compared to the size of the effective area and to d, the distance between the flat surface and the actuators.

These assumptions hold relatively accurately for small deformations.

Consider the forces acting on a small part of the surface of the mirror. Fig 3.1 details the structure of the dynamical behaviour of the membrane under the load P projected on the two planes (yOz) and (xOz) of a three dimension system with its origin in O.

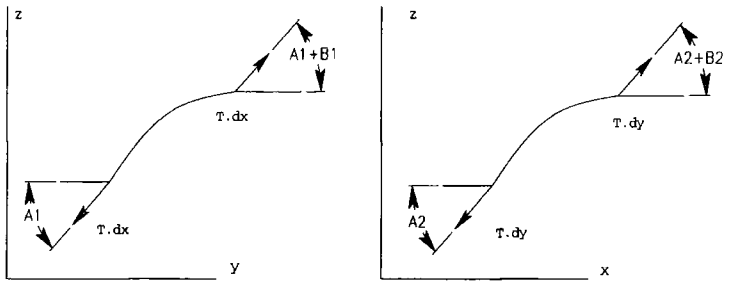

Figure 3.1: Dynamic of the membrane

The horizontal components of the forces are the product of the applied load by the cosine of the angles of inclination. As the angles are considered to be small, the cosine are close to 1. The vertical components keep their angle terms and as the sine of the angle are small they can be replaced by the tangents. The resultant of the horizontal force is small and the horizontal displacements are thus negligible. The actual movement of the membrane is then vertical, along the z axis, under the effect of the vertical components resultants. As the system is in a steady state, the pressure P is balanced by the resultant force due to the elasticity of the membrane. The general equation can then be written:

$$Tdx(A_1 + B_1) - Tdx(A_1) + Tdy(A_2 + B_2) - Tdy(A_2) + Pdxdy = 0 \tag{3.1}$$

where

$$A_1 = \frac{\partial S}{\partial y}$$

$$A_2 = \frac{\partial S}{\partial x}$$

$$B_1 = \frac{\partial^2 S}{\partial y^2} dy$$

$$B_2 = \frac{\partial^2 S}{\partial x^2} dx$$

after simplification one finds the Poisson equation:

$$\frac{\partial^2 S}{\partial y^2} + \frac{\partial^2 S}{\partial x^2} = -(\frac{P}{T}) \tag{3.2}$$

One can now apply the result to the particular case of the Micro Deformable Mirror.

3.2.2 MDM membrane

If V_n voltages are applied on the membrane modelled by a two dimensional grid of N actuators, the surface is deformed. The distance between the actuators and the chip is called d. The tension T on the membrane leads to a deflection of the mirror membrane. This deflection, as we have described above, is supposed to be much smaller than the maximum deflection, so that the electrostatic pressure does not depend on the membrane deformation [1]. The Z-component of the membrane deflection S(x,y), in a linear case, is described by the classical Poisson equation:

$$\Delta S(x,y) = \frac{P}{T} \tag{3.3}$$

where P is given by [6]

$$P = \frac{\epsilon\epsilon_o V(x,y)^2}{d(x,y)^2} \tag{3.4}$$

V is the voltage applied on the membrane, d the distance between the surface and the actuators. The solution of this equation is not simple in our case because the boundary conditions are not trivial. Instead of looking for the exact result the finite difference method has been developed and applied to our case [23]. It is an approximation of the surface by dividing it into a number of small shells in order to write a series of equations and a series of boundary conditions for each shell then for the whole surface. The grid is composed of a number of squares with equal size δ in the X and Y directions. The grid knots are indexed as i and j for X and Y directions. The grid approximation of the Laplace operator can be written:

$$\Delta S = S_{i+1,j} + S_{i-1,j} + S_{i,j+1} + S_{i,j-1} - 4S_{i,j} \tag{3.5}$$

If we combine Equations 3.3 and 3.5, we find the general expression of the membrane

deformation $S_{i,j}$:

$$S_{i,j} = -\frac{1}{4}(\delta^2 \frac{P_{i,j}}{T} - S_{i-1,j} - S_{i+1,j} - S_{i,j+1} - S_{i,j-1}) \tag{3.6}$$

If the expression of the pressure $\frac{P_{i,j}}{T}$ is known, it is easy to find the deflection in each point of the membrane and also to construct a complete model of the mirror for simulations.

Another important parameter to work out is the actual dynamical behaviour of the electrostatic actuators: their repeatability, precision, frequency response and robustness. The same development has been done in detail [6] using the entire theory of elasticity for a flexible, finite solid.

The classical Poisson equation (Equation 3.3) was the basis of the calculations of our results shown in Sections 3.3, 3.4 and 3.5. The two models described above are merely here for reference. We derived our data from Equation 3.3 after verifying that all the assumptions made in Section 3.2.1 were satisfied.

3.2.3 Results

The experiments are based upon the characterisation of the key parameters introduced earlier (e.g the good optical quality of the membrane, initial aberations of the device that we will have to correct before using the MDM as a light modulator, and finally its frequency response). The following paragraph described the warm results for these parameters.

Optical quality

The membranes are fabricated on a single wafer. This process allows the fabrication of up to 16 membranes on the same wafer (made with very high precision) with an optical quality reaching $\sim\lambda/15$ rms ($\lambda = 0.633\mu m$). The flatness of each surface is measured by interferometric techniques [1]. The 19-channel mirror we used has an optical quality of $\sim\lambda/13$ (measured using the *Zygo* interferometer), at warm temperatures and without any tension on it (no voltage applied).

Fig 3.2 shows three interferograms of the surface of the MDM at warm temperatures taken using a *Twyman-Green* interferometer (interferograms from G.Vdovine et al., 1996).

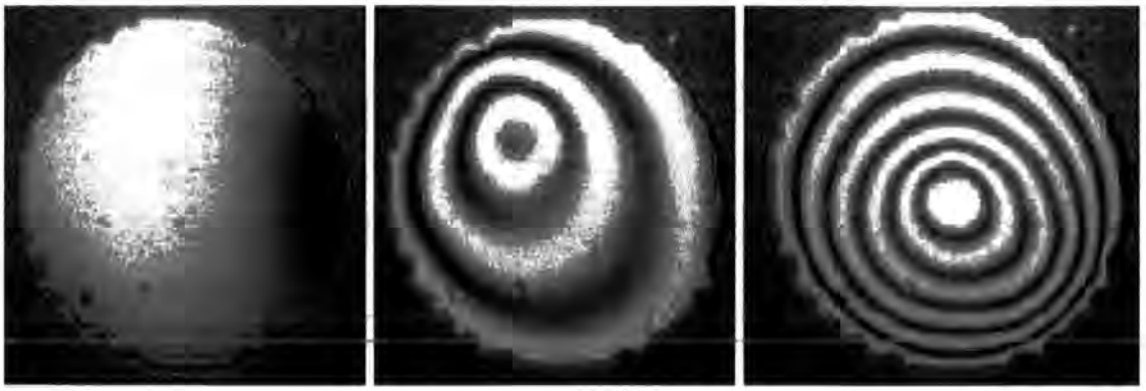

Figure 3.2: Three interferograms of the surface of the 10mm diameter MDM at 290K. The left picture shows the flat surface, the middle picture the surface with a voltage applied on a channel of the inner ring and the third picture gives the surface under tension due to a voltage on channel 1 (centre).

Frequency response

The frequency response of an AO mirror should extend up to at least 1khz (at short wavelengths $\lambda < 1\mu m$ to compensate for atmospheric blurring (because an atmospheric cell will 'change' characteristics with a frequency of 1khz in average). Some experiments run by Gleb Vdovine[1] have shown that the frequency response of the membrane is cut off at frequencies lower than its resonant frequency in vacuum due to the air damping (which can be reduced by making a vent on the electrode to allow air flow). The expressions and values of the resonant frequencies can be found in [20]. In the case of a square membrane (10mm $\times$ 10mm), the theoretical frequency cut off is around 3000Hz for a 100μm air gap between the membrane and the electrodes, and around 50Hz for a 20μm air gap. Fig 3.3 shows the intensity fluctuations, measured using a photodetector, of the mirror to a 25Hz input signal. The input signal of 25Hz initialised the electrodes so that the membrane focused on a point (here on the photodetector) and then defocused so that the variations in the intensity of the signal could be measured. Equation 3.4 shows the dependence of the pressure on the air-gap. As it decreases the force acting on the membrane increases and lower voltages are needed; but the pressure on the membrane becomes high and increases the overall stiffness of the surface. With a compromise between the air gap and the shape of the membrane, the MDM is able to run at any frequency within the range 0...2kHz, which in terms of AO in the visible region is far enough as the typical required value at atmospheric pressure is 1kHz.

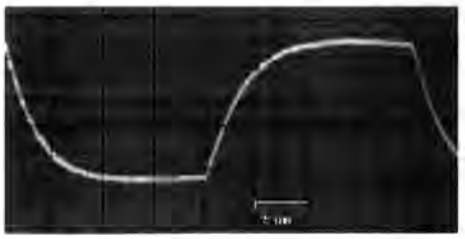

Figure 3.3: Response of the mirror to a 25Hz input signal. One horizontal graduation represents 5ms.

Initial aberrations of the device

However, the shape of the membrane and its physical characteristics induce aberrations which are inherent to the device or caused by external load, electrostatic or mechanical.

Tilt: The first two degrees (x-plane and y-plane) of aberrations are naturally part of the initial deformation of the optical device. It is, however, very easy to remove them by tilting the device on a 2-axis mount.

Defocus: The mirror is particularly interesting if used to produce defocus. The surface changes shape under the influence of the tension, and becomes a parabola (when all actuators recieve the same voltage). The effect of defocus can be controlled. Although the shape gets close to the parabola, it is also subject to the non-uniformity of the air gap (the surface not being perfectly flat) and of the tension applied which induces the next two aberrations.

Coma: The deflection sensitivity depends on the distance between the electrodes and the membrane. The membrane has a very low sensitivity to temperature variations and, in a reasonable range, the deflection due to the temperature changing can be neglected (the amplitude of the aberration does not reach 0.08μm, with a 4.5μm maximum stroke, it represents less than 2%). However, when a voltage is applied to the surface, the membrane has asymmetrical coma-like aberration. It was found ([1] and [21]) that the aberration is caused by a non-uniformity of the air gap.

Spherical: The spherical aberration is produced by the non-uniformity of the tension due to the non-uniformity of the thickness of the membrane. The membrane model developed earlier makes the assumption of a uniform tension but the appearance of this aberration

proves that the tension is higher in the centre. It has been shown that the amplitude of the aberration is much less than the coma-like aberration and so can be neglected as well [1].

Astigmatism: The membrane is attached to a mount. In order to reduce the mechanical stress the die containing the flexible membrane is fixed to the carrier in a small area located far from the optical surface. As we will see later, astigmatism is then created because of this contact with the support.

Summary

Although the membrane is subject to all the first order aberrations, it is relatively stable in terms of its shape: it has a high optical quality and can be selected with a σ up to $\lambda/16$. The key design point is that of compromising the air gap between the electrodes and the membrane as it gives either a good voltage sensitivity with high forces driving the membrane (small air gap) or a high frequency range (big air gap thus smaller forces, membrane less stretched). In our case, we will use a range of 0...100V with a gap of $200\mu m$ which leads the MDM to a linear amplitude response in the frequency range of 0...2kHz.

3.3 Zero point drift

The zero point drift of a thin membrane, and in general of any deformable mirror, is the tendency of the membrane to loose its flatness under any variations of the surrounding conditions (pressure, temperature). This is a major problem to solve since the flatness of the mirror is usually a reference taken to correct for the effects of the atmosphere. In the case where the zero point drift of the device is important, it is necessary to define a reference either by using the surface at given conditions or by calculating the input on the actuators needed to recover the flatness. If the membrane were to change shape with temperature (other parameters like pressure, bias being set), assuming that the central region is of usable optical quality and that the voltage sensitivity of the electrodes is good enough (see Equation 4.2), it would be possible to recover the flat surface (within $\lambda/13$, $\lambda = 0.633\mu m$) after calculating the nominal values of the voltages needed.

3.3.1 Conditions and procedure

The air of the cryostat was pumped out, the vacuum reaching 1.4×10^{-4}mbar at room temperature. The membrane was illuminated by the laser beam behind the CaF_2 window.
In this section, two steps were taken in order to test the zero point drift of the MDM: no voltage applied and then the membrane biased. The procedure is as follows:

Initialisation Each time the experimental setup is switched on, a safety program is run in order to limit peaks, short-circuits, everything that could cause the membrane to catastrophically fail. This program is called *start.prj* (Appendices 5.2.1). It provides a series of questions and delays that reduce the number of human mistakes and more important initializes all the voltages to zero before any operations start.

Experiment Starting at room temperature, the membrane was slowly cooled down by filling the liquid nitrogen bottle. A set of 200Ω resistors was glued on to the top plate of the MDM. They first permitted a very accurate control of the temperature at a certain stage (see Appendices 5.4.3.) for the temperature control as a function of time of experiment; they also provided 25W (for 4h) which was a better way of warming up the entire dewar, quicker than the natural heat loss of the dewar. Once this stage was reached and the temperature stabilised, a series of 7-10 measurements of the peak-valley value of the surface was taken using *Zymod* phase analyser. The software allowed aberrations to be subtracted. Knowing that the mirror naturally has some astigmatism and x-and-y tilt [1], it was possible to remove these aberrations and only take into account the shape variations. This procedure was repeated until the temperature limit was reached. This limit was determined by the heat loss of the dewar introduced earlier. It is typically 90K (see the calibration of the dewar in Appendices 5.4.2). It turned out that the physical limit was more around 115K which leaves an uncertainty regarding the capacities of the membrane at very low temperatures. The 2π steradiants of heat flow from the walls reaching the mirror was responsible for this effect. Solutions to this problem include cold stops and re-imaging optics which would lead to colder temperatures.
However, the amplitude, the range of temperature considered, and the evolution of the results suggest that the MDM behaviour should improve as the temperature gets lower.
In the case of the biased membrane, the main PC controlled the shape of the MDM by

using a program called *bias100V.prj*. It biases the membrane at 100V by initialising all the channels to 100V one by one.

Once the test finished, a program called *end.prj* (Appendices 5.2.5) was run to initialise all the channels to zero.

3.3.2 Results

Two tests following the same procedure were undertaken first using the membrane loose, in other terms no voltages were applied to it, secondly the membrane was biased to a fixed voltage for all channels.

Loose membrane

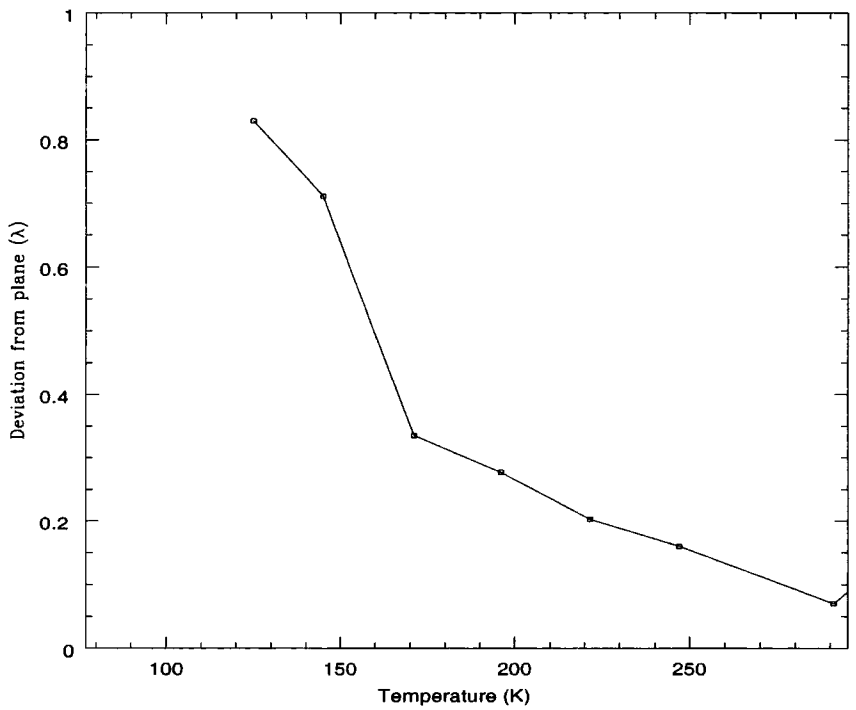

Figure 3.4: Deviation (in $\lambda = 0.633\mu m$) from the plane of the free membrane. The mirror is flat within $\lambda/13$.

The membrane is not under external load, no voltage is applied to it. It can be seen (Fig 3.4) that the deviation increases as the temperature drops. The initial P-V deviation from the plane was 0.070λ, which is less than 0.05μm. As the temperature goes down, the tension

deviation(λ)	0.071	0.166	0.162	0.277	0.336	0.706	0.825
temperature	291	247	231	196	171	146	126

Table 3.1: data of the deviation from the plane of the free membrane.

increases and the membrane looses its flatness. However, the maximum deviation is less than λ (0.633μm), which is very stable considering that the membrane is under no external constraints. The whole MDM is automatically biased to 0.4V by contact with the DC boards, but this bias is minimal.

Biased membrane

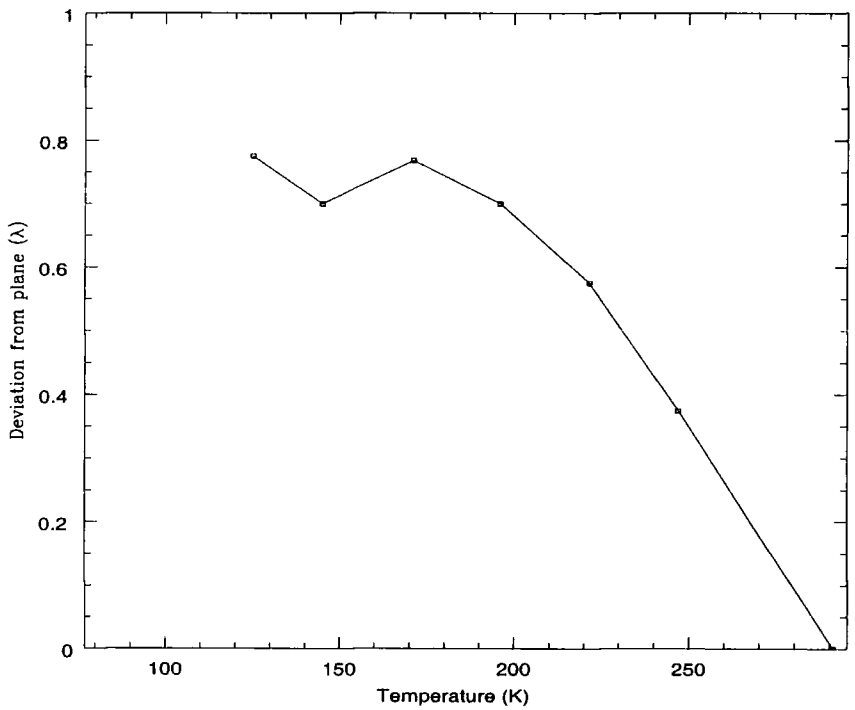

Figure 3.5: Deviation (rms) from the plane of the biased membrane. Here, the value of the deformation is determined after having subtracted the initial biased surface for each measurement (1.405λ). The initial biased surface is the surface at 291K.

The membrane is now under an external voltage. The bias was set to 100V (103V due to the experimental errors on the measurement of the voltage and more specifically due to the poor precision of the power supplies (See Appendices 5.4.4 for the plot of real-to-measured

deviation(λ)	0	0.371	0.572	0.701	0.764	0.700	0.772
temperature	291	247	231	196	171	146	126

Table 3.2: data of the deviation from the plane of the biased membrane.

voltages)). In this case it was easier to subtract the original plane from the consecutive planes at the different temperatures. The results are then the value of the deviation from the plane assuming that the surface at room temperatures was perfectly flat. The only reason for the subtraction is that the shape of the mirror is close to a parabola as the membrane acts like a defocus optical device.

Again, the deviation from the plane increases as the temperature drops. Due to the non-uniformity of the tension, the centre of the membrane gets deflected more than the edges and the membrane turns into a parabolic mirror.

3.3.3 Conclusions

There is a small thermal effect on the membrane. The flat surface, at room temperature, changes shape as the cryostat is filled. The reason is that the tension decreases (see Fig. 3.7) and the deviation in the center is greater than at the edges. However, the maximum deviation reached here for 125K is still under 0.5μm for the biased membrane, which is 11% of the maximum stroke. There is another reason for the variations of the surface. In Section 3.4.2 (Fig 3.8) we discuss the evolution of astigmatism with temperature. It was clear that the natural aberation of the mirror increased as temperature dropped. In order to verify this hypothesis another top plate was made changing the geometry of the contact on the glass wafer supporting the membrane. No quantifications of the results were produced but it was clear that astigmatism was a function of the geometry of this contact. Several conclusions can be drawn out of this little experiment. First the small zero point drift is caused by mechanical stress due to the temperature control stage verified by changing the geometry of the contact. Secondly, before using the mirror with temperature control we cooled it down and visually observed the evolution of the membrane flatness. These observations reinforced that fact that the zero point drift was mainly due to the physical contact with the membrane as nothing was signicantly happening with temperature dropping. Thus, the possibility of building an all-silicon mirror would not bring any major improvement on the matter: the main problem resides in the mechanical

contact. The main conclusion is then that the flatness of the membrane is very little affected by the thermal expansion of the surrounding materials. The tension variations on the surface can be neglected.

3.4 Response and maximum stroke

3.4.1 Conditions and procedure

When assessing a new AO device it is important to determine its response to various conditions (temperature variations, load on the surface, its place in a system). As we have seen in the introduction, the maximum stroke is a key characteristic of such a device because it determines the amplitude of correction reachable with it. The aim of the following test was to draw a good understanding of the membrane response under different loads and more specifically to calculate the value of the maximum deviation. When the deviation is measured, it is the tension applied on the surface that is measured. The aim of this section is then to measure the variations of the tension at different temperatures.
The setup of the experiment is the same as the previous one. The vacuum is done down to 1.5×10^{-4}mbar. However, the procedure is slightly different.

Initialisation All the voltages are initialised to zero.

Experiment Channel 2, from the inner ring of electrodes, was chosen for the sets of measurements. Each time the temperature was stabilised, the voltage was increased by 10V until the limit of 250V was reached. This set of measurements was then repeated until the temperature limit. The difficulty of the experiment lay in the fact that the measurements of the P-V took a long time, which means that the membrane had to be thermally stable for at least 20 minutes.

3.4.2 Results

Tension vs voltage

The tension was calculated using Equations 3.3 and 3.4, with d=200μm. Table 3.3 (Fig 3.6) gives the results of the tension on the membrane as a function of the voltage where three main sections can be drawn out.

0-50V: The membrane is loose. The tension is not balanced and the vertical component is negligible. The voltage applied is just sufficient to stretch the membrane, and the tension increases. As described in the previous section as the temperature goes down

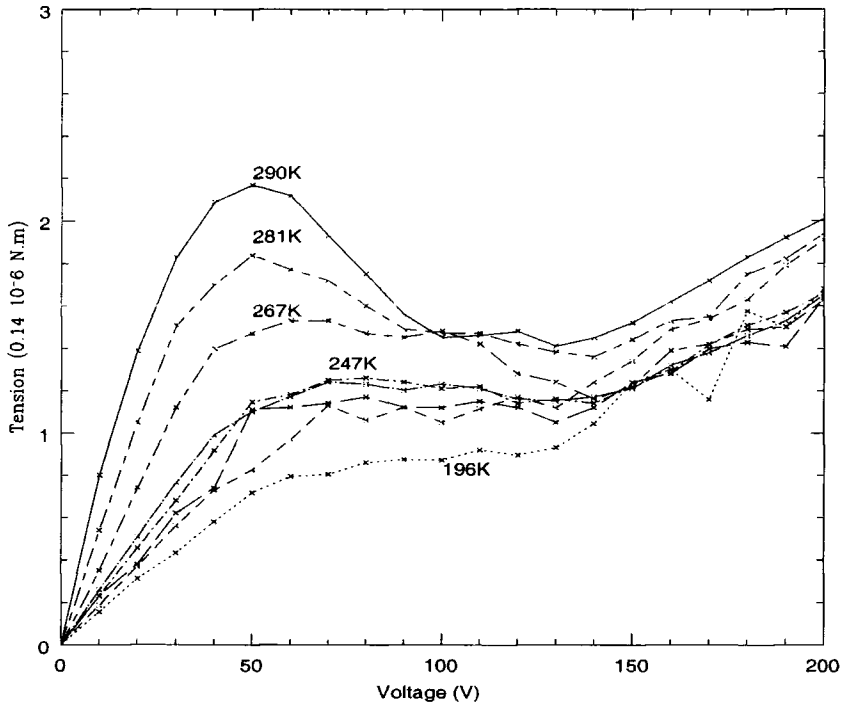

Figure 3.6: Tension on the membrane as a function of the voltage at different temperatures. The temperatures are as follows: 290K-281K-267K-247K-234K-221K-206K-196K. There is a factor of 0.14 on the values of the tension as the distance between the actuators and the membrane varies from one device to the other and they have been calculated for the case of d=200μm. Three ranges can be drawn out: 0-50V where the membrane is loose, 60-130V the *working range* and finally 130-200V the inelastic range.

the membrane gets looser for the main chip shrinks and the perimeter of the boundaries becomes smaller. The "free" membrane is then not perfectly flat. The main abberation of the mirror is initially its astigmatism with a bit of tilt and spherical. This initial deflection can be corrected by mean values of voltage using the entire array of electrodes. After the peak around 50V the tension stabilises and the membrane enters the elastic range.

60-130V: The tension tends to stay constant as the elasticity compensates the increment of internal energy from the deflection process. This range is then defined as the *working range* within which the membrane acts like the perfect membrane model introduced earlier under a linear stress. The load on the membrane is linear at each stage so that the surface is in equilibrium.

V	T(290K)	T(281K)	T(267K)	T(247K)	T(234K)	T(221K)	T(206K)	T(196K)
0	0	0	0	0	0	0	0	0
10	0.8	0.54	0.35	0.25	0.23	0.23	0.18	0.16
20	1.30	1.05	0.74	0.51	0.46	0.38	0.37	0.31
30	1.83	1.51	1.12	0.76	0.68	0.62	0.56	0.43
40	2.09	1.7	1.4	0.99	0.92	0.74	0.73	0.58
50	2.17	1.84	1.47	1.1	1.15	1.11	0.82	0.72
60	2.12	1.77	1.53	1.17	1.18	1.12	0.97	0.79
70	1.93	1.72	1.53	1.24	1.25	1.14	1.13	0.80
80	1.75	1.6	1.47	1.23	1.26	1.17	1.06	0.86
90	1.56	1.49	1.45	1.2	1.24	1.12	1.12	0.87
100	1.45	1.47	1.48	1.23	1.21	1.12	1.05	0.87
110	1.46	1.47	1.42	1.21	1.22	1.15	1.15	0.92
120	1.48	1.42	1.28	1.16	1.14	1.12	1.17	0.89
130	1.41	1.38	1.24	1.15	1.16	1.05	1.18	0.93
140	1.45	1.36	1.16	1.17	1.14	1.12	1.24	1.04
150	1.52	1.44	1.22	1.21	1.22	1.24	1.34	1.24
160	1.62	1.53	1.39	1.32	1.29	1.28	1.49	1.3
170	1.72	1.55	1.42	1.38	1.42	1.4	1.54	1.16
180	1.83	1.75	1.49	1.46	1.52	1.43	1.63	1.76
190	1.92	1.82	1.5	1.53	1.57	1.41	1.79	1.50
200	2.01	1.94	1.63	1.65	1.66	1.64	1.91	1.68

Table 3.3: Values of the tension T (10-6 N.m) as a function of the voltage (Volt) applied to the membrane at different temperatures.

130-200V: The membrane is now in the inelastic range. Its thickness decreases from the center as the load increases. If the *shear stress* σ is assumed constant within this range (which remains to be proved), the force acting on the membrane goes like σ/R. The tension grows linearly until the fraction point.

Tension vs temperature

T (10-6 N.m)	1.68	1.51	1.3	1.2	1.07	1.08	1.11	0.93	0.75	0.56
$< T >$ (10-6 N.m)	1.73	1.71	1.49	1.27	1.26	1.18	1.04	1.85	0.66	0.5
temp.(K)	290	281	267	247	232	221	206	196	147	131

Table 3.4: Data of the average tension $< T >$ (calculated over the range [30-170V] for each temperature) and the value of the tension T for an 80V load on channel 2.

We have now reached the certitude that the membrane is safe at very low temperatures. As

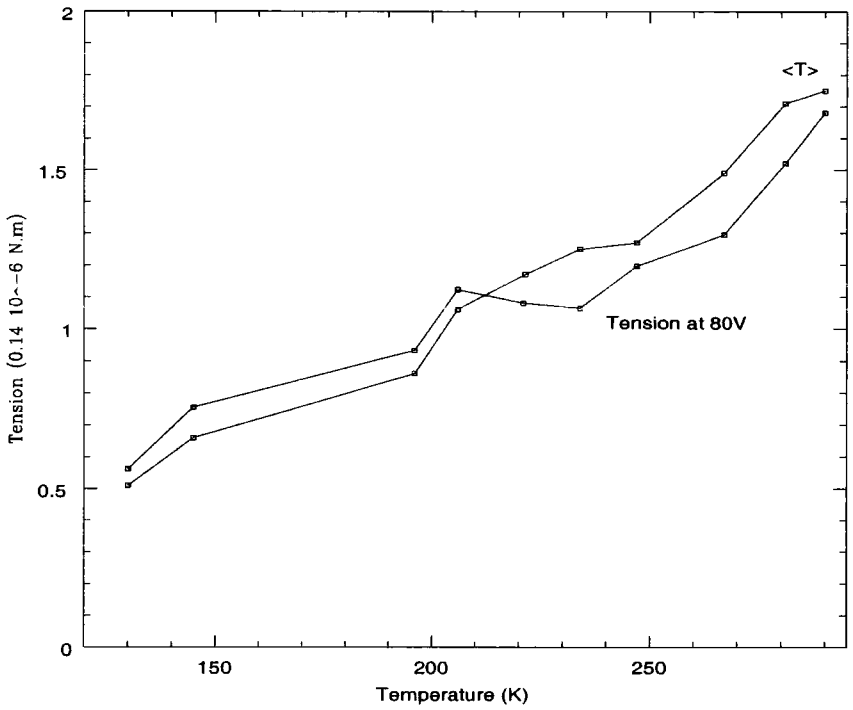

Figure 3.7: Tension applied on the surface as a function of the temperature. $< T >$ is the average value of the tension calculated over the 16 values from a range slightly larger [30-170V] than the working range [60-130V] defined earlier. The other curve is the value of the tension when an 80V load is applied on channel 2. The tension in both cases was calculated using Equation 3.4.

the temperature decreases, the tension on the surface also decreases. This can be explained by looking at the thermomechanics of the MDM. The membrane is mounted over an aluminium coated glass plate, on top of a PCB board. The contraction of the silicon nitride membrane is negligeable (the coefficient of thermal expansion of the silicon is very small: $2.5K^{-1}$ against 12 for aluminium). The process is symmetrical so that the centre of the membrane stays at the same place, but the radius of the membrane gets smaller due to the tension from the wafer. The result is that the membrane gets looser.

There is an important drawback to this phenomenon. The glass wafer is attached to the PCB board in two points. As the two materials also have again different expansion coefficients, the mechanical tension increases in these two particular points. This leads to an increasing astigmatism with temperature dropping. It was however very difficult to differentiate between the aberration caused by this compression and the physical contact between the top plate and

the glass wafer by means of the indium disc. One solution would be to attach the glass wafer to only one fixed point and thus allow thermal contraction.

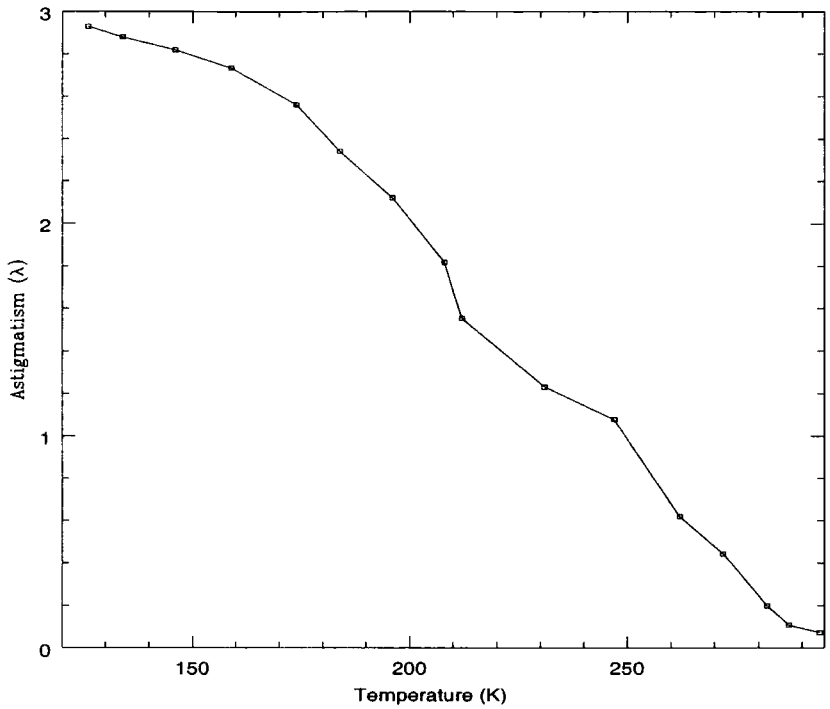

Figure 3.8: Astigmatism caused by the mechanical contact between the glass wafer and the temperature plate.

The critical design part is then to be found on the thermal contact between the membrane and the temperature plate. Fig 3.8 illustrates the effects of the mechanical tension due to the springs (see Appendices 5.1.2 Fig 5.6 for pictures of the components).

Conclusions

This series of tests has shown that the MDM is perfectly able to work under cryogenic conditions. It has also shown the difficulty of the experiment: the control of the temperature of the membrane. The design of the contact, circular, conical..., is critical, and in order to do further studies of the surface evolution it will be critical to design different thermal contacts. The MDM is ideal when it is a question of eliminating low degrees of aberrations, but it is also very easy to induce some of them like tilt, spherical and astigmatism by making any contact. The size of the device is an advantage but it leads to a much higher sensitivity to any physical

contact. The ideal solution would be to control the temperature of the membrane without having to touch it.

3.5 Dynamical response

3.5.1 Conditions and procedure

The third and final test run on the MDM determined the dynamical response, in other words how the membrane stiffness changes with the temperature, and thus how its elasticity under load varies with temperature. The distance between the membrane and the actuators, which we quoted earlier in the introduction to the MDM as a key design factor, is not taken into account. The purpose of this series of experiments is to quantify the variations in the frequency response by measuring the intensity fluctuations of the reflected beam.

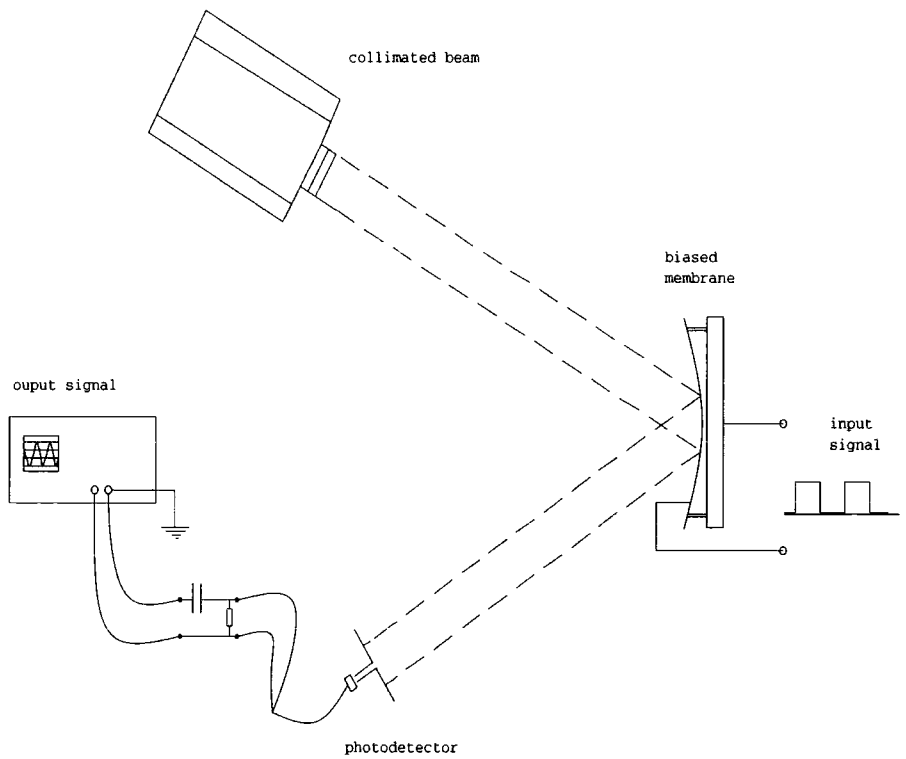

Figure 3.9: Setup of the experiment. The laser shoots on the 50V biased MDM which recieves an input signal initialising the voltages to 130V and then returning values to 50V. The variations in the intensity of the reflected beam are detected by the photodetector which then transmits the signal to the oscilloscope where the output from the mirror is measured.

Setup The low-pass filter between the photodetector and the oscilloscope was introduced to reduce the high frequency of 1.8MHz noise coming from the main PC (voltage control) card, and a 27KHz coming from the photodetector. The cryostat was under vacuum, the original temperature was room temperature and all the channels were initialised to 0V.

Procedure The dewar is filled with liquid nitrogen and the temperature stabilised. Once the temperature is stable the program *50-130.prj* was run and a series of 10 measurements of the frequency response of the membrane taken.

The membrane was biased at 80V which is in the middle of the working range. The program set all channels to 80V then in a 180Hz cycle set the membrane to 130V transforming the membrane into a defocus device.

The photodetector recieved and transformed the light amplitude variations of the incoming beam into an electrical signal. The oscilloscope allowed us to visualise and measure the variations in the amplitude of the intensity of the beam focused and defocused by the membrane.

The frequency was then directly read on the screen taking into account the experimental uncertainties (noise from the photodetector, vibrations from the surrounding environment, lights). The phase of the beam was not measured for technical reasons and further research should be carried on on that matter.

The same steps were repeated for three input frequencies of 180Hz, 640Hz and 1.64kHz until the temperature limit was reached.

The frequency loops used in the programs were limited by the speed of the data process. Appendices 5.2.4, Fig 5.7.and 5.8 give the calibration of the index loop value.

3.5.2 Results

The same test was run at three different frequencies.

180Hz

The frequency response was very stable. The implications of this result are important. First it implies that the biased membrane is stable under a rectangular input pulse and it does not brake. Second, the membrane keeps its dynamical qualities as temperature drops. The main conclusion is that dynamically, the membrane can support input pulses even under external varying conditions.

There was some uncertainty on the measurement as the noise from the photodetector and from the computer were difficult to remove but the result is precise enough to conclude that at this frequency input the membrane keeps its elasticity.

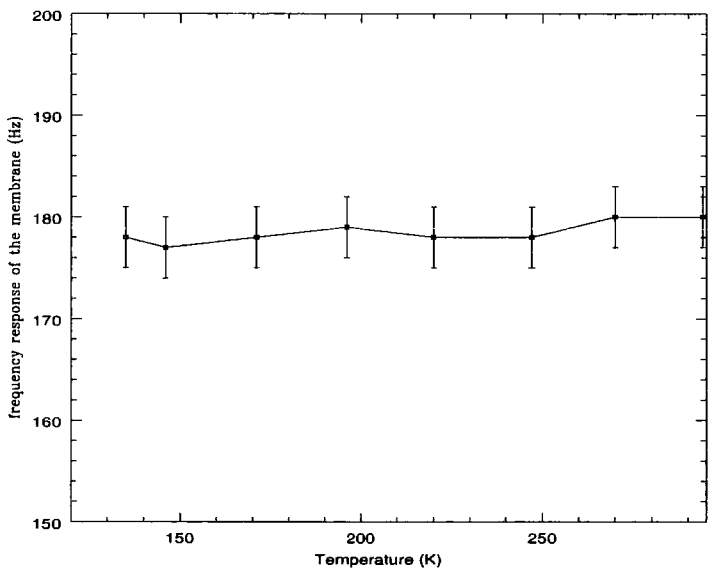

Figure 3.10: Frequency response of the membrane with a 180Hz input signal. The experimental error is ±3Hz. It is due to some noise from the photodetector and was measured on the oscilloscope output.

640Hz

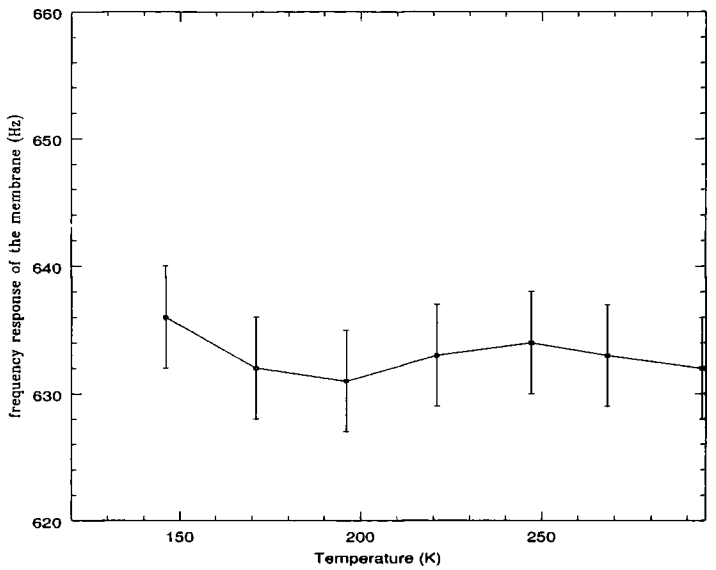

Figure 3.11: Frequency response of the membrane with a 640Hz input signal. The experimental error is ±4Hz.

The same conclusion can be drawn out of this plot. The frequency chosen, 640Hz, is the limit of speed of the program written in C++. It is an adequate value as the typical correction frequency of an AO system is 1kHz.

1.64kHz

In order to make sure the membrane works at higher frequencies a series of tests have been run, with the same procedure as above, but this time in the hope of finding out the breaking point of the membrane. The program consecutively turned all channels on to the value expected. This process took a lot of time and energy. This led to a low frequency limit. In order to increase the speed of the input, a new program was written initialising only the central and inner ring channels. It was then possible to reach frequencies up to 12kHz.

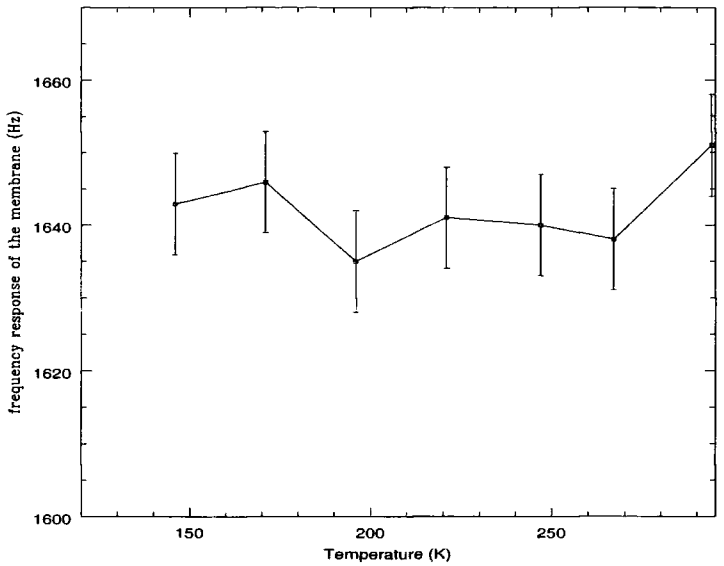

Figure 3.12: Frequency response of the membrane with a 1.64kHz input signal. The experimental error is ±7Hz.

3.5.3 Conclusions

The membrane frequency response is not a function of the temperature, or if it is, it is not significant. The membrane supported very high variations of voltage at all the temperatures, under very high frequencies up to 12kHz. We measured frequency of defocus and not the amplitude of the signal on the photodetector (mainly due to the fact that the laboratory was full of background noise from light sources and power supplies). The amplitude has not been quantified, but it was seen not to be a strong function of frequency. Further work should be done in order to quantify both the amplitude fluctuations with frequency and more importantly the phase of the response.

Chapter 4

Applications and Conclusions

4.1 Applications

4.1.1 HST

The first test images obtained with the Wide-Field Planetary and Faint Object Cameras of the Hubble Space Telescope soon after the launch revealed that the main optics of the telescope suffered from severe spherical aberration. After investigation it was found that the problem was due to a manufacturing error made when the primary mirror was ground and polished. As a result of an incorrectly assembled null lens, the mirror was figured about 2 microns (6λ of spherical aberration at $\lambda = 0.633\mu m$, HeNe laser used to test the mirror) too 'low' at its outer edges. In December 1993, the Maintenance and Refurbishement to HST mission was launched in order to update some instruments (WF/PC II, solar panels) and to install an optical corrective device COSTAR (Corrective Optics Space Telescope Axial Replacement) which restored the two prime scientific objectives of the FOC: deep imagery and photometry of very faint celestial objects and imagery of bright objects at the highest possible resolution available from HST. The cost of the mission: $1 billion including the research put into the device, the cost of the launch and the installation on the telescope. We outlined this event for two reasons. Firstly, the spherical aberration of the primary mirror could have been corrected by means of an Active Optics system. However, the question of cost is still fundamental, which leads us to the second point: A small, light weight device, with a stroke range of 0-5μm. The MDM has been seen to be a very good optical corrector for low order aberrations. In terms of HST defects, it would

have suited the situation by both correcting the daily fluctuations of the structure (in the order of a few nm) and the manufacturing errors (in the order of a few μm).

4.1.2 Space Active Optics. NGST

Active Optics

While the adaptive optics concept is the same for ground based and for space telescopes, its implementation in space and on the ground are very different. Ground-based AO systems are designed to remove the time-varying phase errors introduced by atmospheric turbulence. They then require a bandwidth of a few hundred Hz. On the other hand Space Active Optics are used to correct the fabrication errors or misalignment due to thermal expansion. They then only need a frequency range of a few mHz. Table 4.1 gives the main differences between the two devices.

Table 4.1: Comparison between Active and Adaptive Optics.

	Ground based (D=10m, r_0=20cm)	Space
Number of actuators	2500	300-1200
Actuator stroke	10μm	50nm
Actuator resolution	10nm	0.1nm
frequency range(Hz)	100-800	0.001 Hz

The daily update of the position of device X and Y in space requires a simple and inexpensive Active Optics system that can be launched in space without much energy (weight is money) and meets all the requirements of low temperature techniques. The Micro Deformable Mirror, as we have seen, answers all of these points. It works under cryogenic temperatures, weighs virtually nothing and measures less than a match box.

Table 4.1 shows that the actual corrections on the structures in space are less than 100nm, with an ideal actuator resolution of 0.1nm. The resolution of the membrane is voltage applied and air gap dependent. It will then strongly depend on the accuracy of the distance between the actuators and the membrane as well as on the accuracy of the power supplies used to feed the mirror. It is relatively easy to produce such power supplies and this problem should not be regarded as a limitation in the applications of the MDM. The other problem can be avoided by biasing the membrane with high voltage. It will stretch it and put a tension on it so that

the resolution on the voltage applied is increased. The force, produced by each electrode in the case of biasing, is defined as

$$F = \frac{\epsilon\epsilon_0(V_b + V)^2 s}{d^2} \tag{4.1}$$

where V_b is the bias and V the voltage applied, it is easy to see that the sensitivity to the control voltage V is given by

$$\frac{dF}{dV} = \frac{2\epsilon\epsilon_0 V_b s}{d^2} \tag{4.2}$$

for $V_b >> V$. d (200μm) is the gap between the electrodes and the membrane, s is the diameter of one electrode (2mm for the 19-channel mirror).

Increasing the bias increases the sensitivity of the device which allows the membrane to be controlled with low-voltage integrated electronics. A typical value of bias voltage which we used in our experiment was 80V as it was in the working range of our device (see Section 3.4.2). The MDM provides a reliable way of correcting low order aberrations with high sensitivity in the voltage control, so it is a good candidate for space applications.

NGST

Following the huge success of the HST, some very ambitious and technologically advanced projects have arisen in the last 2 years. In a report[16], 'HST and Beyond', the Association of Universities for Research in Astronomy (AURA) "urged the development of a general-purpose, near-infrared observatory equipped with a primary mirror larger than 4 meters," that "should operate far from Earth to maintain its cool temperature" (down to 50K). "It should be lightweight and compact" to fit in a middle-size launch vehicle and finally it should be able to adjust the deployment misalignments and the thermal effects.

In order to provide an HST-like resolution in the near-infrared and a wide field imaging, the primary mirror requires a very high optical quality. Different concepts of deployable mirrors have been proposed but all will have the same problems. The optical quality of the fabricated mirror segments should be about $\lambda/30$ (λ being in the visible) over dimensions up to a few cm. This precision is easily achieved on ground based techniques but after petal positioning and focus deviation considerations the main conclusion is that "some form of active figure compensation will be needed for any large, passively cooled mirror".

In this constant low temperature environment, there is no need to control the temperature

variations by direct measurements. The problems encountered on Earth to maintain the MDM at a constant level would be avoided as the whole telescope would be cold. With the high density of actuators and their accuracy, alongside a very stable dynamical behaviour at cryogenic temperatures, the MDM is the best candidate for the NGST requirements of a small, reliable Active Optics device.

4.2 Conclusions

In previous research[1] for tilt correctors and scanners, the MDM has shown very good reliability for improvement of the contrast ratio and picture quality. Its optical quality reaches on average $\lambda/15$ and a peak to valley in the order of λ=0.633μm. The natural aberrations amplitude, tilt, astigmatism, spherical and coma when used as a defocus, does not reach λ and they can easily be removed. The influence functions of the membrane can be described by the set of polynomials introduced in Appendix 5.5, the Zernicke polynomials. Combining all these characteristics, the first conclusion was to consider the MDM as a potential candidate for AO. The new technologies in the world of Instrumentation open the doors to a new area: cryogenic AO instruments. The idea is not new but its applications are. The main purpose of this thesis was to show the suitability of the MDM for cryogenic conditions: How its characteristics, maximum stroke, dynamical response , change with temperature; what are the problems encountered with such techniques and how they can be solved in order to make the MDM an *ideal* low-temperature device.

The membrane has been shown to work. A total of 25 cycles from 290K to 125K have been done. And the optical quality of the membrane has not changed. This was a fear: how the whole device would react under such drastic conditions. But we showed that the surface does not significantly change its shape with temperatures (these variations can be corrected for with a bias). It is stable within 0.5μ. The air gap between the membrane and the actuators does slightly change as the tension decreases but the very simple membrane model developped in chapter 3 remains relevant. The maximum stroke is constant (with a biased membrane at 80V) at 4.5μm , with a small increase as the temperature goes down due to the small movement of the surface. The dynamical response is not affected by thermal variations and the membrane

can support frequencies up to 12kHz (although more work needs to be done in order to quantify the amplitude variations of the signal at different frequencies). Any external contact, thermal, mechanical or vibrational, would disturb the shape of the membrane, but it is a very safe, reliable piece of technology.

The main problems we encountered were mostly design problems with the pieces that hold the MDM in place in the dewar, the heat loss of the thermal system dewar-MDM and more specifically the thermal contact between the cold plate and the mirror. It was fundamental to be able to control the temperature inside the dewar. We did that by glueing a set of diodes and a set of resistors on a specially designed plate that was in mechanical contact with the aluminium coated glass wafer through an indium disc. It appeared that this contact was the source of astigmatism (up to 2.5λ) and that it was difficult to remove it. A future avenue of research will be to control the temperature of the membrane without having to touch it. There is, however, a problem inherent to the mirror: the different materials used on the device (PCB, Aluminium, silicon) are thermally incompatible. We suspect this mixture is responsible for thermal stress and thus small shape changes. It is possible, however, to create an all glass device (Technologies developed by Gleb Vdovin) which would eliminate the stress due to the contact between two different materials.

To sum up, the membrane gets slightly looser with decreasing temperature but it can be considered stable within 0.5μm. The only significant stress comes from the structure of the device itself and from any piece added on top of it.

In terms of the MDM itself, the epoxy glue that was first used on top of the membrane aluminium coated mount tends to pull off the aluminium coating. To avoid this problem, a 3-piece plate was made and the components were glued on the top plate. Further work on cold clamping is needed.

In addition to the problem of glueing temperature sensors to the membrane, the main conclusion is that a gold coated mirror mount would be better than the aluminium coated wafer which did not resist big thermal amplitudes. Gold coating is the best candidate for stronger soldering and more scientifically for infrared purpose as it offers a higher coefficient of reflection than aluminium (it is used on the coating of secondary mirrors of big telecopes).

The MDM works under cryogenic conditions and meets all the requirements of an AO system.

Acknowledgments

The list of people I would like to thank is very long and I am sure to forget half of them. But I am particularly thankful to:

Madeleine, for your love, your support this entire year and for your help on this document.

Gleb Vdovine, for the free mirrors which we have tested.

Mark Chang, for your patience when answering my numerous questions and for your very practical help at solving my problems.

Bernie, for your advice and help during this year, in many aspects of the work and for delicious international meals.

The Instrumentation Group, Roger, Sylveszter, John Webster, Gordon, David, Richard, James, our friends the engineers, Robert.

The YTA, keep cool!

Et bien sur ceux qui me sont chers:

Mes parents qui m'ont beaucoup soutenus tant spirituellement, moralement, professionellement que financierement, Guillaume, Florence et Magali.

Mike and Rosemary for their support, welcoming house and the wonderful english food.

Julian and the Wednesday lunches. I have forgotten a lot of people involved in my year at very different levels but to all thanks a lot.

Chapter 5

Appendices

5.1 Designed pieces

The following pieces have been designed to install the MDM inside the dewar and to control the temperature at its surface. The research included designing all the pieces, machining them and testing them to match the requirements of the experiments.
The whole device is composed of four main components which technical drawings are shown in the following sections: the L-bracket fixed on the cold plate of the dewar and the temperature control plate divided in three independant components. All pieces were made with tolerance of 1mm and the design of this aluminium-G10 MDM holder appeared to work perfectly well.

5.1.1 L-bracket

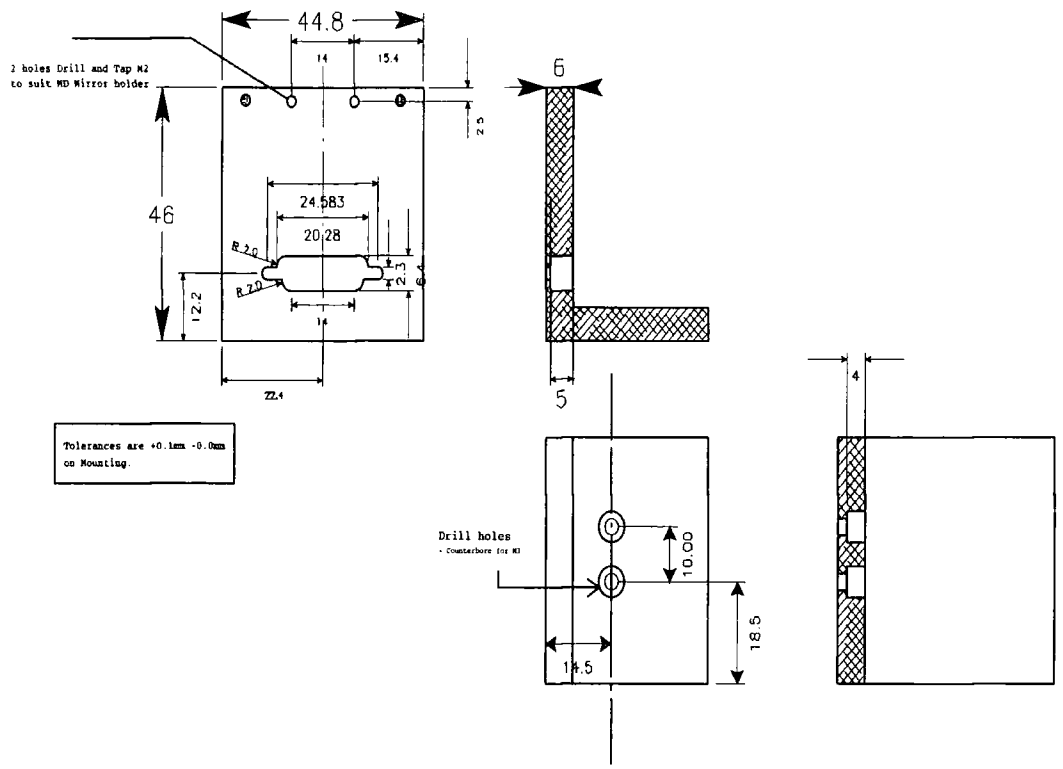

Figure 5.1: L-bracket in aluminium. This piece is in contact with the cold plate of the bottle and thus plays an important part in the thermal efficiency of the whole device. It has been tested and found close to the 85K. It is not a thermally limiting part.

5.1.2 3-piece glue plate

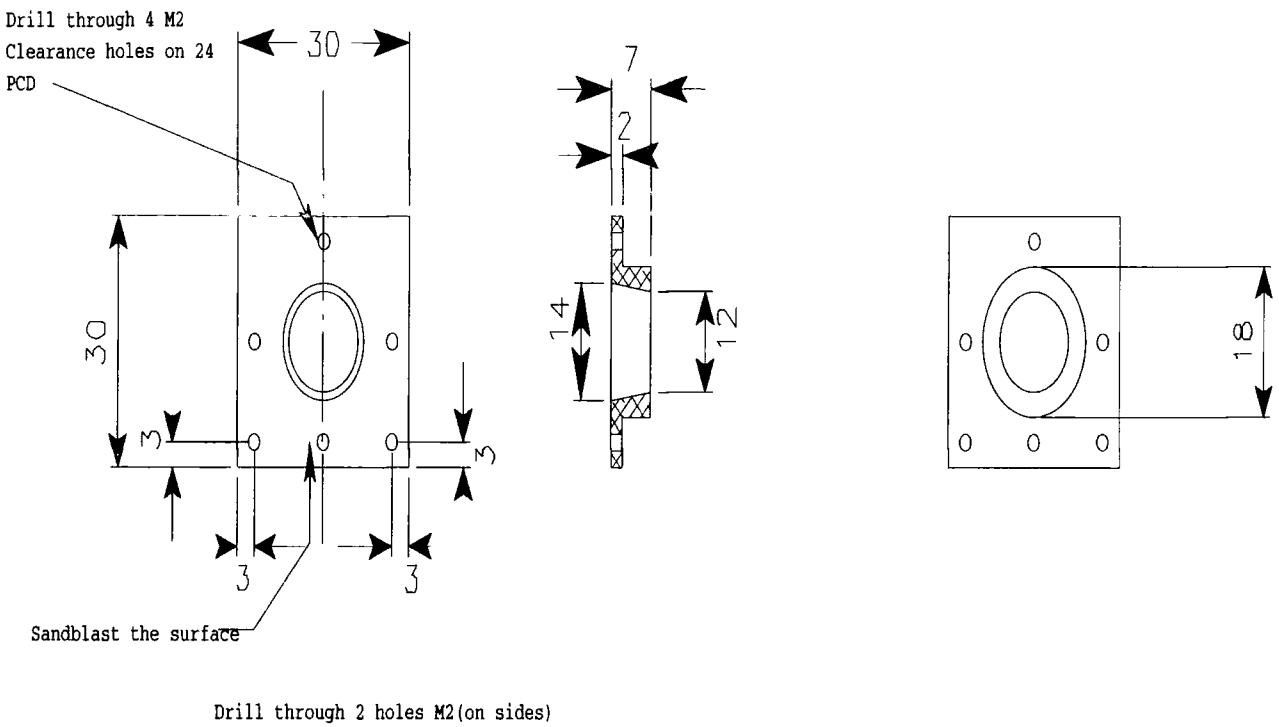

Figure 5.2: Technical drawing of the circular top plate.

4 Corner holes: Drill through M2

3 internal holes: Drill and Tap M2,
3 mm deep
+ air hole for each

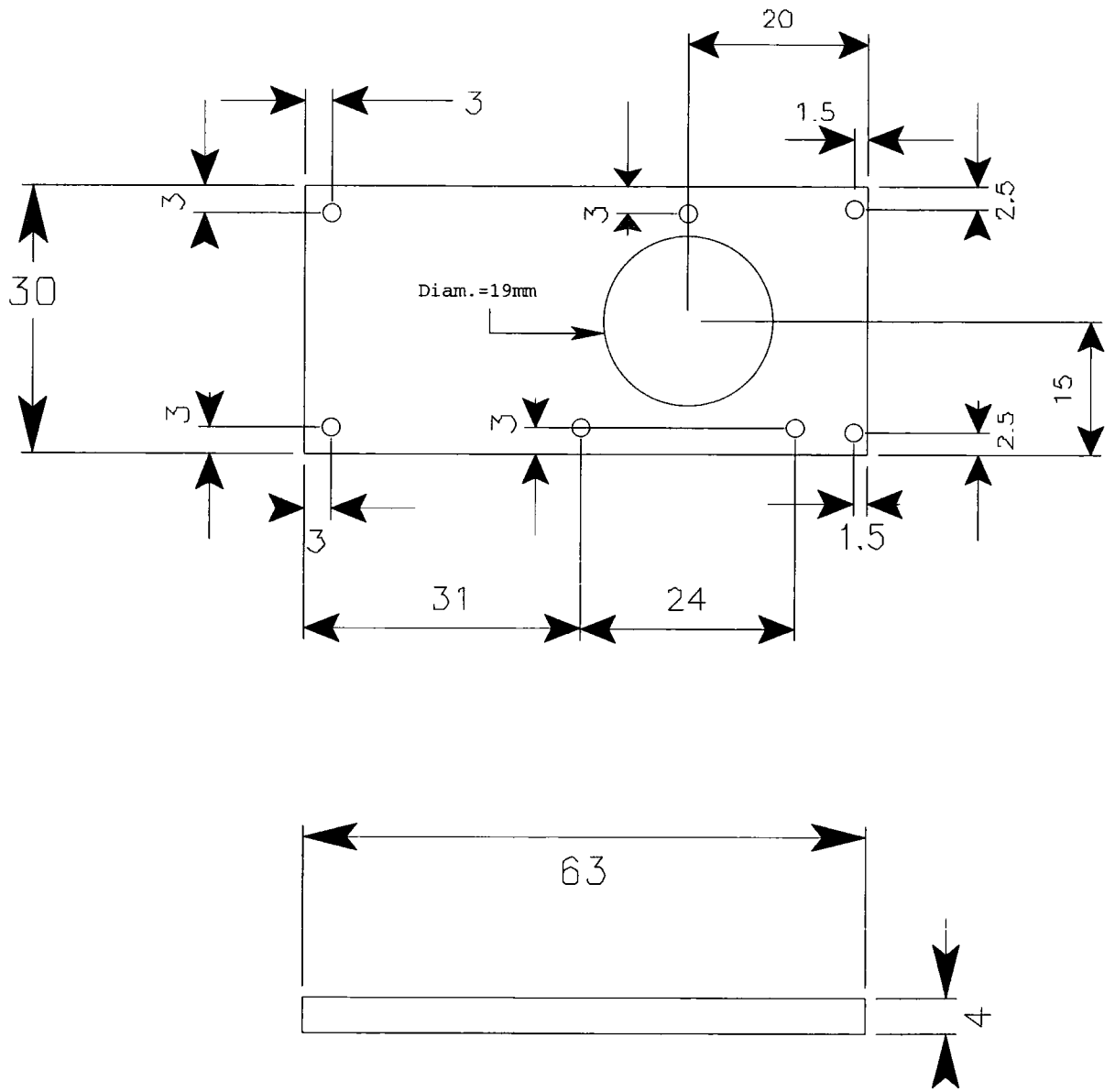

Figure 5.3: Technical drawing of the middle plate.

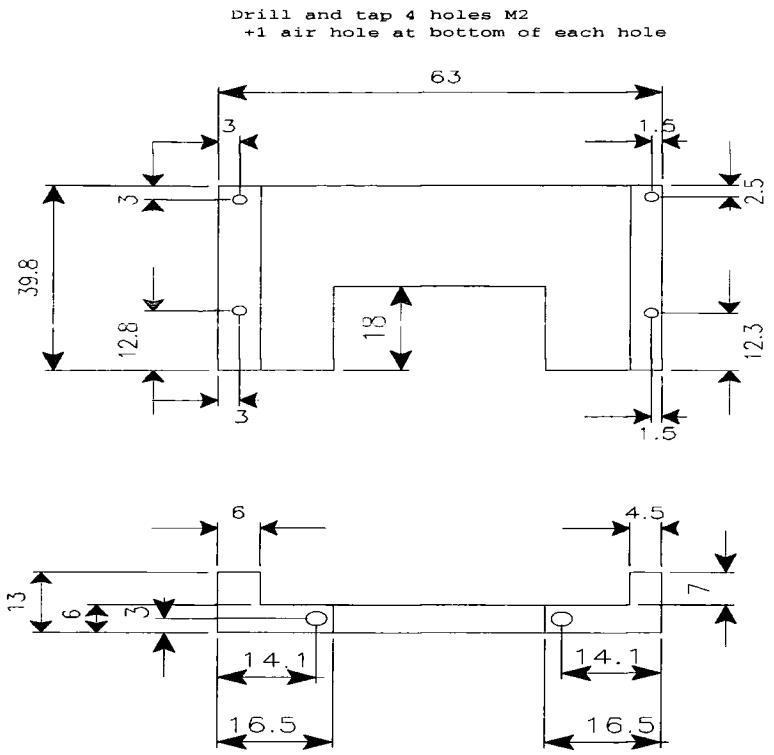

Figure 5.4: lower plate. The top and lower pieces are made of aluminium for its density and its high thermal conduction. The middle is a thermally non conductive plate in PCB. The advantage of having three separate pieces is that it is then possible to refabricate one of them. The top plate is in contact with the aluminium coated glass wafer by means of an indium disc. This contact induces mechanical stress on the wafer and produces astigmatism. In order to verify the stress due to the mechanical contact, several top plates have been made with different contact geometries (circular and semicircular). It appeared clear that the source of aberrations was this contact as the P-V of astigmatism was a function of the temperature and of the contact used.

Figure 5.5: Set of pictures detailing the sequence of mounting the MDM on the cold MDM holder. From left to right, the aluminium L-bracket, the aluminium mount, the PCB mount were all designed to recieve the MDM and to work under cryogenic conditions. The fourth picture shows the thermal contact (ring of indium) between the glass wafer and the top plate holding the electronic components. Air holes have been drilled through to avoid any added mechanical load on the device between the structure and a screw due to trapped air. The PCB board on which the MDM is fixed is attached at only two points to the low plate to minimise the mechanical stress at low temperatures. The fifth picture shows the top plate in aluminium holding the electrical components. The components were glued on the surface using epoxy glue, thermally conductive glue, to avoid any loss in the thermal contact with the membrane.

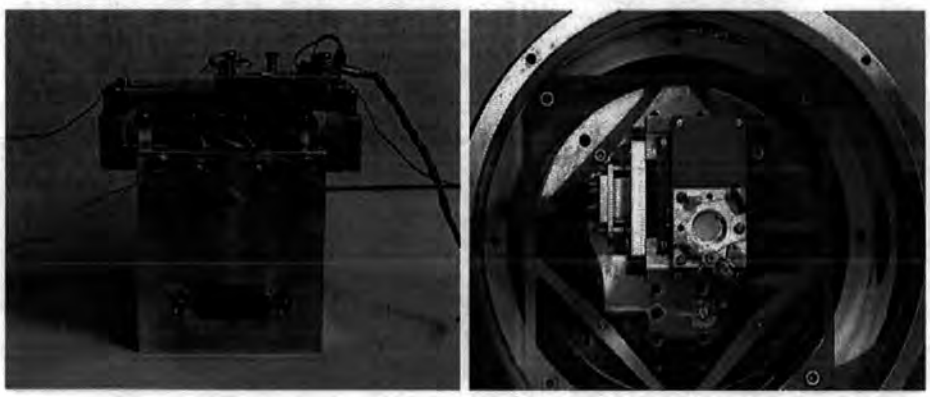

Figure 5.6: The MDM is ready to be installed inside the dewar. The connections to the outside are made by cryogenic wires, thin and insulated wires. The heat loss through these connections is minimal.

5.2 Voltage control and safety programs.

All the following programs have been written under the Symantec C++ Environment for DOS. The advantage of this environment was to be able to create projects containing a program core with the required function alongside libraries and headers common to all of them. As only the small 19-channel mirror has been used, only one board address was included in the listings but all programs are compatible with the addition of the second board.
Their order of appearance follows the general procedure of an experiment.

5.2.1 am.h

Header file for the **am.lib** library. By B.J.Rauscher.

```
/* AOS sys defs */
#define N_CHAN  19              /* Number of channels in AOS */
#define DACS_PER_BD 20          /* Number of DACs per board */
#define DAC_LOW_LIM 0           /* DAC low voltage limit */
#define DAC_HIGH_LIM 255        /* DAC high voltage limit */
#define BASE_L  0x380           /* Base address of low mem DAC board */
#define BASE_H  0x3A0           /* Base address of high mem DAC board */

/* define Viglen arrow keys */
#define UP_ARROW  18432
#define DN_ARROW  20480
#define L_ARROW   19200
#define R_ARROW   19712

/* Declare addr[] and voltage[] arrays. These are
        defined in set_dac.c */
extern const int addr[];
extern int voltage[];

/* Function templates... */
extern int set_dac(void);
extern void delay(int);
extern void error(char*, char*);

/* End of header */
#endif
```

5.2.2 start.c

This program provides a set of warnings and resets all channels to 0V before switching on the high power supply. By S.Bonicel.

```
#include <stdio.h>
#include <stdlib.h>
#include <dos.h>
#include <bios.h>
#include <ctype.h>
#include "am.h"
```

```
main()
{  char ans1,ans2,ans3,ans4,rep;
   int i,value[20];
   printf("\n You are starting the program reminder \n");
   printf("\n Press return to continue\n");
   scanf("%c", &ans1);
   printf("\n Verification of connections : \n");
   printf("\n *Grounds* \n");
   printf("\n *Power supplies* \n");
   printf("\n *Power supplies-Boards* \n");
   printf("\n *Boards-Boards *\n");
   printf("\nHave you finished the first step?\n");
   printf("\nThen press return to continue\n");
   scanf("%c", &ans2);
   printf("-------------------------------------------------------------------------");
   printf("\nwithout applied voltage the surface of the mirror should be at 0V, which
   printf("-------------------------------------------------------------------------");
   printf("\n\n");
   printf("\nYou can now put the power supplies on, in this order:\n");
   printf("\n* +15V *\n");
   printf("\n* -15V *\n");
   printf("\n If you have finished wait 30 sec and press return \n");
   scanf("%c",&rep);
   printf("-------------------------------------------------------------------------");
   for (i=0; i<=N_CHAN; i++)
    { voltage[i]=0;
      set_dac();
    }
   printf("\n\n");
   printf("\nYou have now set all the voltages of the boards to 0V\n");
   printf("\n\n");
   printf("\n* +V High *\n");
   printf("-------------------------------------------------------------------------");
   printf("\nNo change should appear on to the surface of the mirror. Check with Zygo
   scanf("%c", &ans4);
   printf("\n When you finish press a key to continue\n");
   printf("-------------------------------------------------------------------------");
   printf("-------------------------------------------------------------------------");
   scanf("%c", &ans3);
   printf("\nYou must do all theses steps --in order-- before using the mirror, otherw
   return(0);
   }
```

5.2.3 mytest8.c

It controls the integer values sent to the main board driving the 19 channels, checking that channel 0, the membrane, is never called (to avoid any short circuit).

```
#include <stdio.h>
#include <stdlib.h>
#include <dos.h>
#include <bios.h>
#include <ctype.h>
#include "am.h"

/* define global variables */
int key;        /* key most recently pressed */

/* The heart of the matter... */
int main(void)
{
   int i;                                  /* Convenient counter index */
   int num;                                /* Holds current channel number */

    /* Initialize all DACs to zero to avoid damaging equipment */
    for (i = 0; i <= N_CHAN; i++) voltage[i] = 0;
    if (set_dac() != EXIT_SUCCESS) {
        error("main", "illegal voltage detected! No change made.");
    }

    printf("Control channel voltages using RIGHT and LEFT arrows\n\
    UP swtiches the channel, DOWN stops the program\n");
    printf("NumLock should be off\n");

    /* Simple command parser. This is an infinite loop */
    for (;;) {

        /* Outter infinite loop handles channel number */
        printf("Input channel number ->");
        scanf("%d", &num);
        while (num < 1 || num > N_CHAN) {
                printf("Out of bounds! Input channel number again ->");
                scanf("%d", &num);
        }
        /* Inner infinite loop handles inc and dec of voltage
           also detects exit conditions. */
        for (;;) {

            /* Fetch a new keystroke */
            key = bioskey(0);
            /* printf("%d\n", key); */

            /* Test and handle voltage inc */
            if (key == R_ARROW) {
                voltage[num] += 5;
                if(voltage[num] > 255 ) voltage[num]=255;
                if(voltage[num]<0 ) voltage[num]=0;
                printf("Channel %d = %d\n", num, voltage[num]);
            }

            /* Test and hangle voltage dec */
            if (key == L_ARROW) {
                voltage[num] -= 5;
                if(voltage[num] > 255 ) voltage[num]=255;
                if(voltage[num]<0 ) voltage[num]=0;
                printf("Channel %d = %d\n", num, voltage[num]);
            }
```

```
            /* Update voltages */
            if (set_dac() != EXIT_SUCCESS) {
                        error("main", "illegal voltage detected! No change made.");
                        }
            /* Detect move to next channel */
            if (key == UP_ARROW)  break;
            /* Done? */
                if (key == DN_ARROW)  exit(0);
                }
    }
        return(EXIT_SUCCESS);
}
```

This program calls the $set - dac()$ function which updates the voltages and checks the channels called to avoid channel 0.

```
void set_dac(int voltage[19], int value[19])
  { int i,port;
    for (i=0; i< DACS_PER_BD; i++)
     { port=BASE_L + addr[i];
       value[i]=voltage[i];
       outp(port,value[i]);
     }
    for (i=DACS_PER_BD;i< N_CHAN; i++)
     { port=BASE_H+ addr[i];
      value[i]=voltage[i];
      outp(port,value[i]);
    }
```

See **am.h** for the definition of the variables.

channel	board output	address	membrane actuator
0	0	23	membrane(bias)
1	10	13	1
2	4	19	2
3	7	16	3
4	12	11	4
5	15	8	5
6	18	5	6
7	2	21	7
8	5	18	8
9	6	17	9
10	8	15	10
11	9	14	11
12	11	12	12
13	13	10	13
14	14	9	14
15	16	7	15
16	17	6	16
17	19	4	17
18	1	22	18
19	3	20	19

Table 5.1: The output voltage of the channel N [0...23] of the 8-bit 24-channel DAC board is controlled by sending integer value V [0...255] to the output port BA+N. As an example C operator **outportb(0×300+4, 255);** sets the output voltage to its maximum for the 5th channel of the board whose base address is 0×300. There are two boards whose addresses are respectively 0×300 (DIP position 11100000) for the first board driving channels 1 to 19, and 0×380 (DIP position 11000000) for the second board driving channels 20 to 37, in case the big 37-channel MDM needs to be used. The two boards have been installed on the main frame of the PC and tested. For the purpose of the research only the first board has been used.

5.2.4 test1.c

This program sets all the channels or only a specified number (s) to a bias and using a calibrated j-loop allows an input frequency.

```
#include <stdio.h>
#include <time.h>
#include <stdlib.h>
#include <dos.h>
#include <bios.h>
#include <ctype.h>
#include "..\am_durha\include\am.h"

/* Declare addr[] and voltage[] arrays. These are
        defined in set_dac.c */

const int addr[N_CHAN+1] = \
{23,13,19,16,11,8,5,21,18,17,15,14,12,10,9,7,6,4,22,20};

int voltage[N_CHAN+1] = \
{0,0,0,0,0,0,0,0,0,0,0,0,0,0,0,0,0,0,0,0,0};

int key;
int set_dac(void);

int main(void)
{
  const int DELAY = 0;
  int volt,j, num;
  int i,count=0,s;
  const int loops = 1e6;

    /* Put all channels at 50volt, or any other voltage */
    for (volt= 0; volt <= N_CHAN; volt++) voltage[volt] = 50;
    if (set_dac() != EXIT_SUCCESS) {
        error("main", "illegal voltage detected! No change made.");
        exit(1);
    }

   for (j=0;j<loops;j++) {

      for (s=0;s<=7; s++){
      voltage[s] = 50;
      if (set_dac() != EXIT_SUCCESS) {
        error("main", "illegal voltage detected! No change made.");
        exit(1);
     }
```

```
      }
     /*usleep(100);*/
     /*for (i=0; i<DELAY; i++) count++;*/

    for (s=0;s<= 7; s++) {
    voltage[s] = 100;
    if (set_dac() != EXIT_SUCCESS) {
        error("main", "illegal voltage detected! No change made.");
        exit(1);
     }
    }
    for (i=0; i<DELAY; i++) count++;
    /*usleep(100);*/
    }
  return EXIT_SUCCESS;
}

 int set_dac(void)
{
    int i, port, value;
        int counter;

        for (i = 0,counter++; i < N_CHAN; counter++,i++)

    /* First update low mem board */
    for (i = 0; i < DACS_PER_BD; i++) {

        /* Make sure voltage is within 0-255 limit */
                if (voltage[i] < DAC_LOW_LIM || voltage[i] > DAC_HIGH_LIM) {
                        return(EXIT_FAILURE);
                }

        /* Write to port */
        port = BASE_L + addr[i];
        value = voltage[i];
        outp(port, value);
    }
 return(EXIT_SUCCESS);
}
```

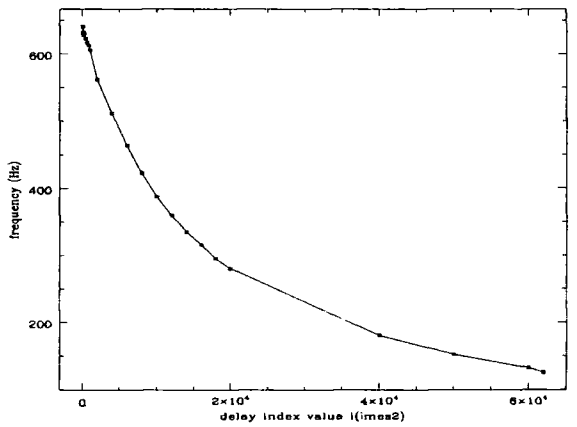

Figure 5.7: Calibration of the j-loop for the entire set of actuators. Two frequencies have been tested: 180Hz and 640Hz the upper limit of the loop.

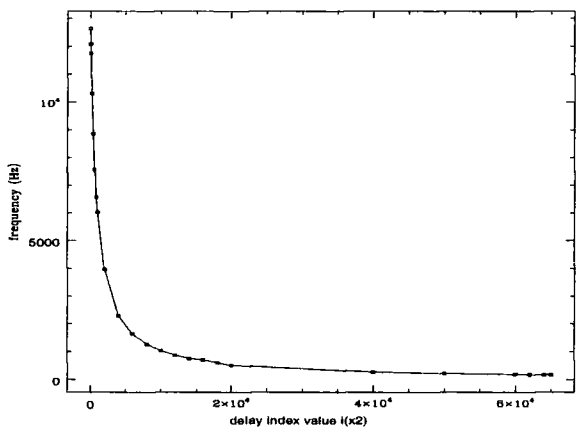

Figure 5.8: Calibration of the j-loop for the channels 1.7 at frequencies 1.8kHz and 12kHz.

5.2.5 end.c

Simple program to proceed safely end the experiment.

```
#include <stdio.h>
#include <stdlib.h>
#include <dos.h>
#include <bios.h>
#include <ctype.h>
#include "am.h"

main()
{  char ans1,ans3;
   int i; /* value[20] */

   printf("\n You are ending your experiments. Follow the procedure. \n");
   printf("\n Press a key and return to continue\n");
   scanf("%c", &ans1);
   printf("\n\n\n");
   printf("\n Switch off the power supplies in this order \n");
   printf("\n \n");

       /*for (i = 0; i <= N_CHAN; i++) voltage[i] = 0;
    if (set_dac() != EXIT_SUCCESS) {
       error("main", "illegal voltage detected! No change made.");
       exit(1);
    } */

    for (i=0; i<=N_CHAN; i++)
    { voltage[i]=0;
      set_dac();
    }
    printf("\n You have reset all voltages to 0V.");

   printf("\n\n\n");
   printf("\n* +V High *\n");
   printf("\n* +15V *\n");
   printf("\n* -15V *\n");
   printf("\n\n\n\n");
   printf("\nYou can close this application and switch the computer off. \n");
   exit(1);
}
```

5.3 Conversion of intensity maps from Zymod

Each *.**INT** file is a uniform array of intensity values stored as single bytes integers. The following program looks for the reference tag in the header of the reference file and creates three subfiles: a raw data file storing the image only; a header file storing the old header; and a *.**FITS** file where the raw data is added to a *.**FITS** header. This program has the merit of creating both a raw data and a *.**FITS** file. It can be converted into a *.**IMG** format in IRAF but this process was not satisfying. The other possibility was to use the raw data (with the ext *.**IMH**) under any display package and convert it into a *.**JPEG** or even an *.**EPS** file. The second method appeared to be the most efficient as either *.**JPEG** or *.**EPS** files are very easy to transfer and compatible with any image packages. The files were then easily transformed.

```
/* =-=-=-=-=-=-=- */
/* reformatZygo.c */
/* =-=-=-=-=-=-=- */
/*************************************************************************/
/* Takes framegrabbed Zygo images, bytestrips the header and             */
/* Assumes there is a subdirectory "floats" to store the output files.   */
/*************************************************************************/
/* Author : Sebastien Bonicel */
/* Date :         13/02/1998  */
/*****************************/

#include <stdlib.h>
#include <stdio.h>
#include <math.h>

main(int argc, char **argv)
{
  int *ZygoArray;
  int *headerArray;
  int x, y, naxis1, naxis2;
  int i, j, byte;
  int day, month, year;
  int headerTag;
  int headerTagMSB;
  int headerTagLSB;
  int headerByte[20];
  int byte_count;
  char name[64];
```

```
char infilename[99];
char outfilename[99];
char hdrfilename[99];
char fitsfile[99];
char response[3];
FILE *inptr, *outptr, *hdrptr, *fitsptr;

/* comment to make sure that this is the right number of arguments */
/**********************/
if (argc != 3) {
  fprintf(stderr,
          "Usage = %s <filename> <end of header tag>\n",
          argv[0]);
  exit(-1);
}

/* Takes command line input and gives it to a variable */
/*******************************************************/
sprintf(infilename, argv[1]);
headerTag = strtoul(argv[2], NULL, 0);

if (headerTag > 0xff) {
  headerTagMSB = 0xff;
  headerTagLSB = headerTag - 0xff;
}
else {
  headerTagMSB = 0;
  headerTagLSB = headerTag;
}
fprintf(stderr,"Header Tag MSB = %d, LSB = %d\n", headerTagMSB, headerTagLSB);

/* Allocate memory for the image */
/*********************************/
headerArray = malloc (128*128*sizeof(*headerArray));
ZygoArray = malloc (10000*sizeof(*ZygoArray));

if (NULL == (inptr = fopen(infilename,"rb"))) {  /* Open Zygo data file */
  printf("Error opening file %s\n", infilename);
  exit(-1);
}
sprintf(hdrfilename,"%s.hdr",infilename);
if (NULL == (hdrptr = fopen(hdrfilename,"wb"))) {  /* Open output header file */
  printf("Error opening file %s\n", hdrfilename);
  exit(-1);
}
sprintf(outfilename,"%s.img",infilename);
if (NULL == (outptr = fopen(outfilename,"wb"))) {  /* Open output image file */
```

```
    printf("Error opening file %s\n", outfilename);
    exit(-1);
  }
  sprintf(fitsfile,"%s.fits",infilename);
  if (NULL == (fitsptr = fopen(fitsfile,"wb"))) {  /* Open output FITS file */
    printf("Error opening file %s\n", fitsfile);
    exit(-1);
  }
  byte = 0; j = 0;
  while (EOF != (ZygoArray[byte] = (int) fgetc(inptr)))
    byte++;                                  /* read in data one byte at a time */
  x = ZygoArray[4];
  y = ZygoArray[6];
  printf("Image size (%d,%d)\n", x, y);
  for (i = 0; i < byte+1; i+=2) {              /* perform byteswap */
    int tmp;
    tmp = ZygoArray[i+1];
    ZygoArray[i+1] = ZygoArray[i];
    ZygoArray[i] = tmp;
  }

  /* Find end of header */
  /**********************/
  j = 0;
  for (i = 0; i < byte+1; i++) {               /* Look for header end tag values */
    if (ZygoArray[i] == headerTagMSB && ZygoArray[i+1] == headerTagLSB) {
      headerByte[j] = i;
      fprintf(stderr,"Header tag value found at byte = %d\n",i);
      j++;
    }
  }
  for (i = 0; i < headerByte[0]+2; i++)
    fputc(ZygoArray[i], hdrptr);

  /* Write image to file in 2 byte integers (byteswapped with respect to the Zygo outp
  /*********************************************************************************
  for (i = (headerByte[0]+2)*2; i < byte+1; i++)
    fputc(ZygoArray[i], outptr);
/* Print the header. Each header line must be 80 char long ( 80*36 lines=2880 bytes).

  fprintf(fitsptr, "SIMPLE   =           T / FITS STANDARD
  fprintf(fitsptr, "BITPIX   =           8 / FITS BITS/PIXEL
  fprintf(fitsptr, "NAXIS    =           2 / NUMBER OF AXES
  fprintf(fitsptr, "NAXIS1   =         %3d /
  fprintf(fitsptr, "NAXIS2   =         %3d /
  fprintf(fitsptr, "ORIGIN   = 'Zygo'      /
  fprintf(fitsptr, "DATE     =             /
```

```
  fprintf(fitsptr, "IRAFNAME =   %s / NAME OF IRAF IMAGE FILE
  fprintf(fitsptr, "IRAF-MAX = 0.0000000E0 / DATA MAX
  fprintf(fitsptr, "IRAF-MIN = 255.0000E0  / DATA MIN
  fprintf(fitsptr, "IRAF-BPX =           8 / DATA BITS/PIXEL
  fprintf(fitsptr, "IRAFTYPE = 'SHORT'     / PIXEL TYPE
  fprintf(fitsptr, "END
  fprintf(fitsptr,"
  fprintf(fitsptr,"
  fprintf(fitsptr,"
  fprintf(fitsptr,"
  fprintf(fitsptr,"
  fprintf(fitsptr,"
  fprintf(fitsptr,"
  fprintf(fitsptr,"
  fprintf(fitsptr,"
  fprintf(fitsptr,"
  fprintf(fitsptr,"
  fprintf(fitsptr,"
  fprintf(fitsptr,"
  fprintf(fitsptr,"
  fprintf(fitsptr,"
  fprintf(fitsptr,"
  fprintf(fitsptr,"
  fprintf(fitsptr,"
  fprintf(fitsptr,"
  fprintf(fitsptr,"
  fprintf(fitsptr,"
  fprintf(fitsptr,"                              ");

  /* Write image to FITS file (byteswapped with respect to the Zygo output) */
  /*************************************************************************/
  byte_count = 0;
  for (i = (headerByte[0]+2)*2; i < byte+1; i++) {
    fputc(ZygoArray[i], fitsptr);
    byte_count++;
  }

  for ( i = 2880 - (byte_count % 2880); i > 0;i--)
    putc(0, fitsptr);
  fclose(inptr);

  fclose(fitsptr);
  fclose(hdrptr);
  fclose(outptr);
  printf("Done.\n");
}
```

5.4 Calibrations of instruments

5.4.1 Diodes

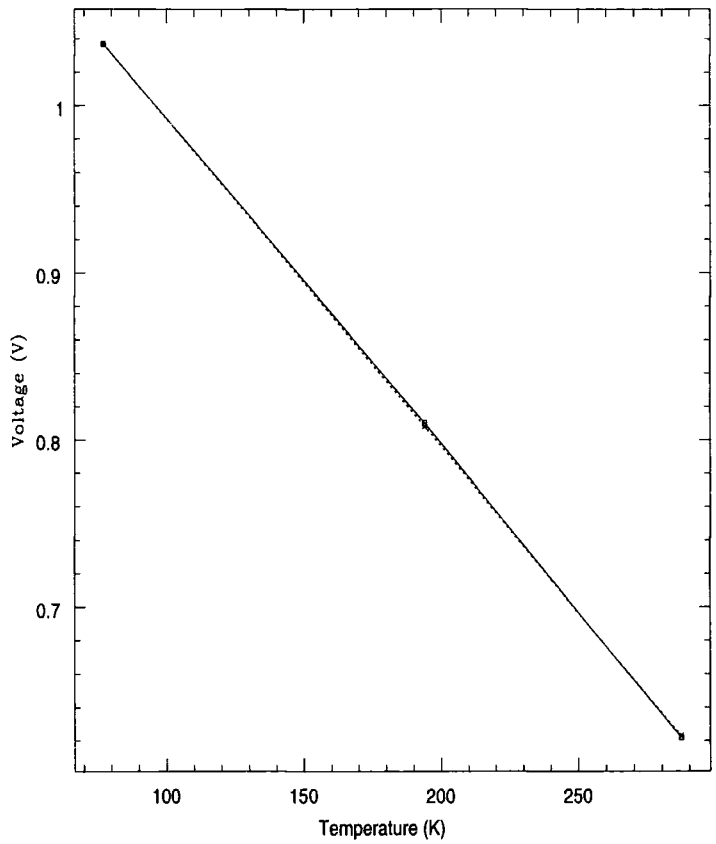

Figure 5.9: Calibration of two similar diodes. They have been glued to the top plate of the MDM holder and served as thermometers. The uncertainty is less than 0.001V which leads to an uncertainty on the measurement of the temperature of ± 0.5K. The two diodes were not used at the same time. Not knowing how the connections, the epoxy and the diodes would behave at low temperatures, it was a security.

5.4.2 Cryostat

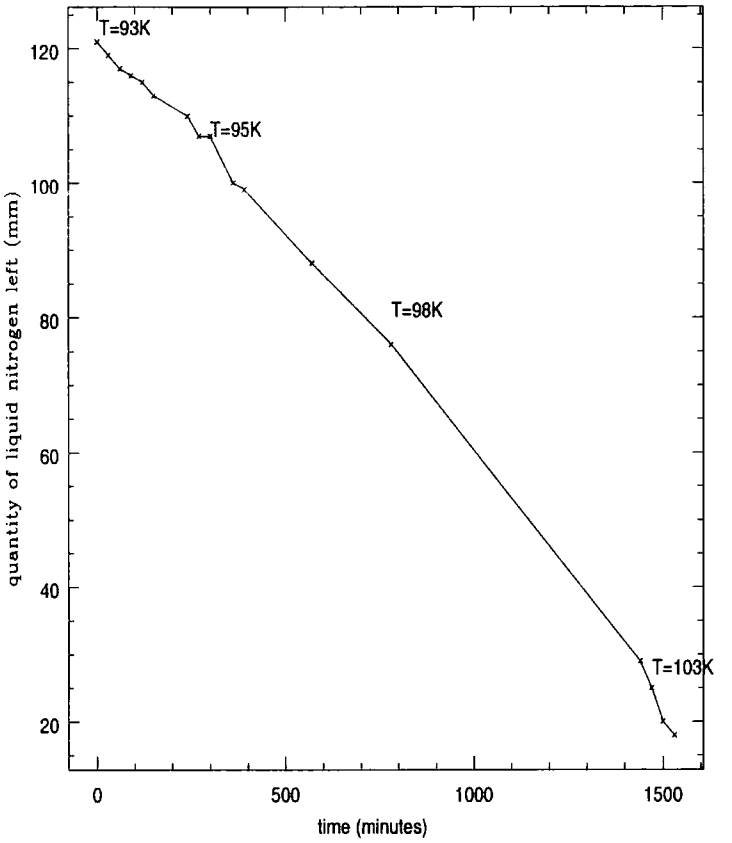

Figure 5.10: Loss of liquid nitrogen in the dewar with respect to time. It should be noted that the bottle contains liquid nitrogen for at least 24 hours. This means that the cold plate stays at a very constant temperature for more than 12 hours. The assumption of neglecting the heat loss during a 20min experiment is therefore accurate.

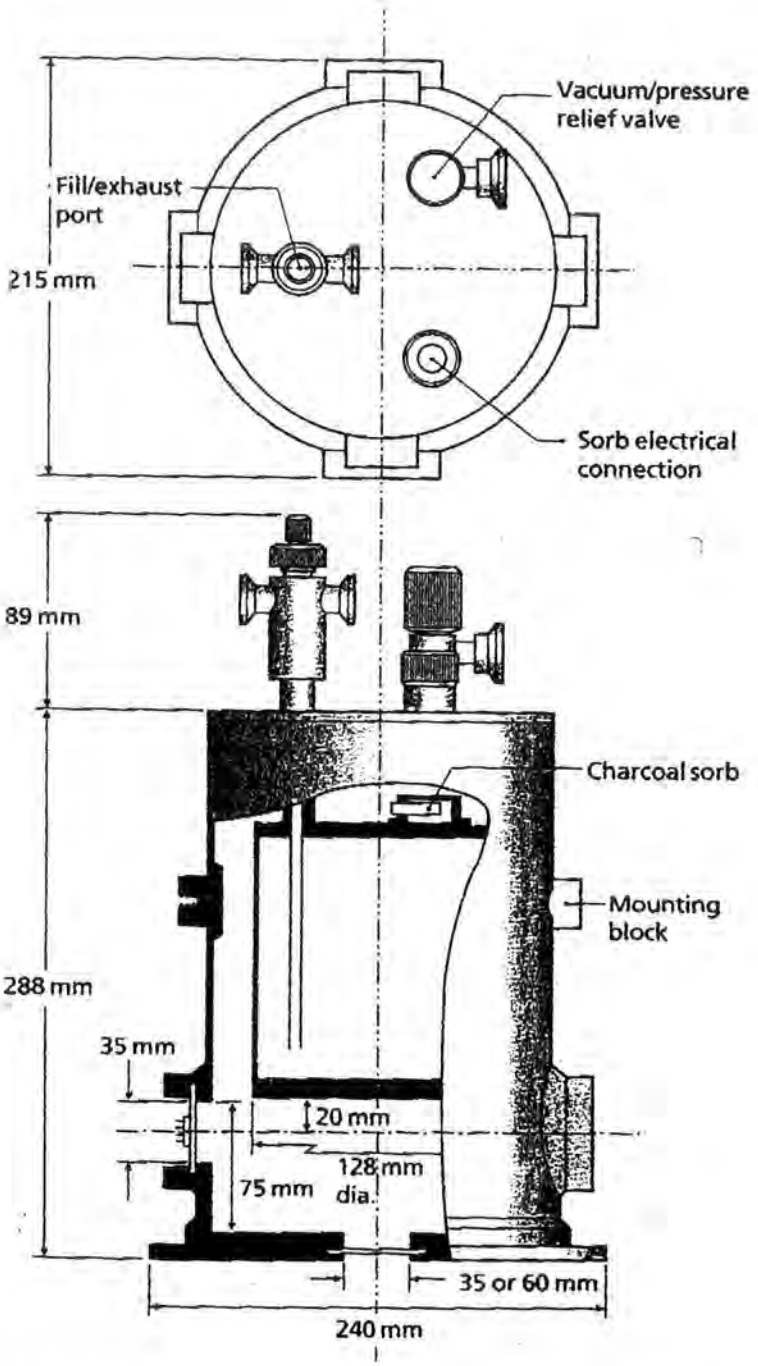

Figure 5.11: Diagram of the cryostat. The advantage of this device is its size; its disadvantages are the heat losses. The exhaust plays a big part in that process as it is in constant contact with the warm room. However, the stability of the dewar was sufficient for the purposes of the experiments.

5.4.3 Temperature stability inside the dewar during an experiment

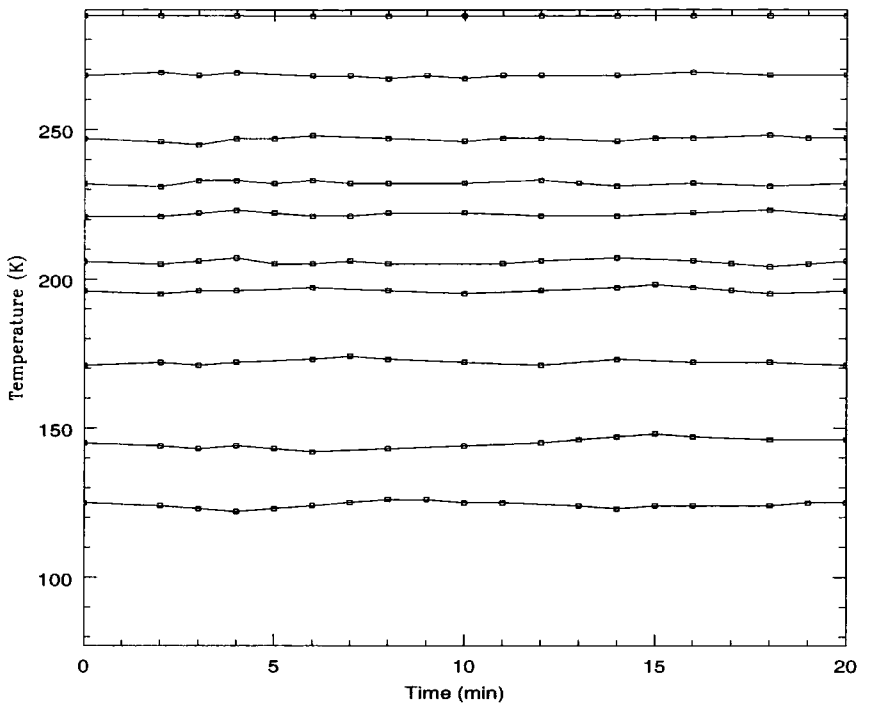

Figure 5.12: Control of the temperature during an experiment. The plot gives the stability of the temperature measured during a 20min experiment. The control was done by using the set of resistors glued on the top plate. The uncertainty of the measurements of the voltage (diodes) is ± 0.5K.

5.4.4 Power supplies

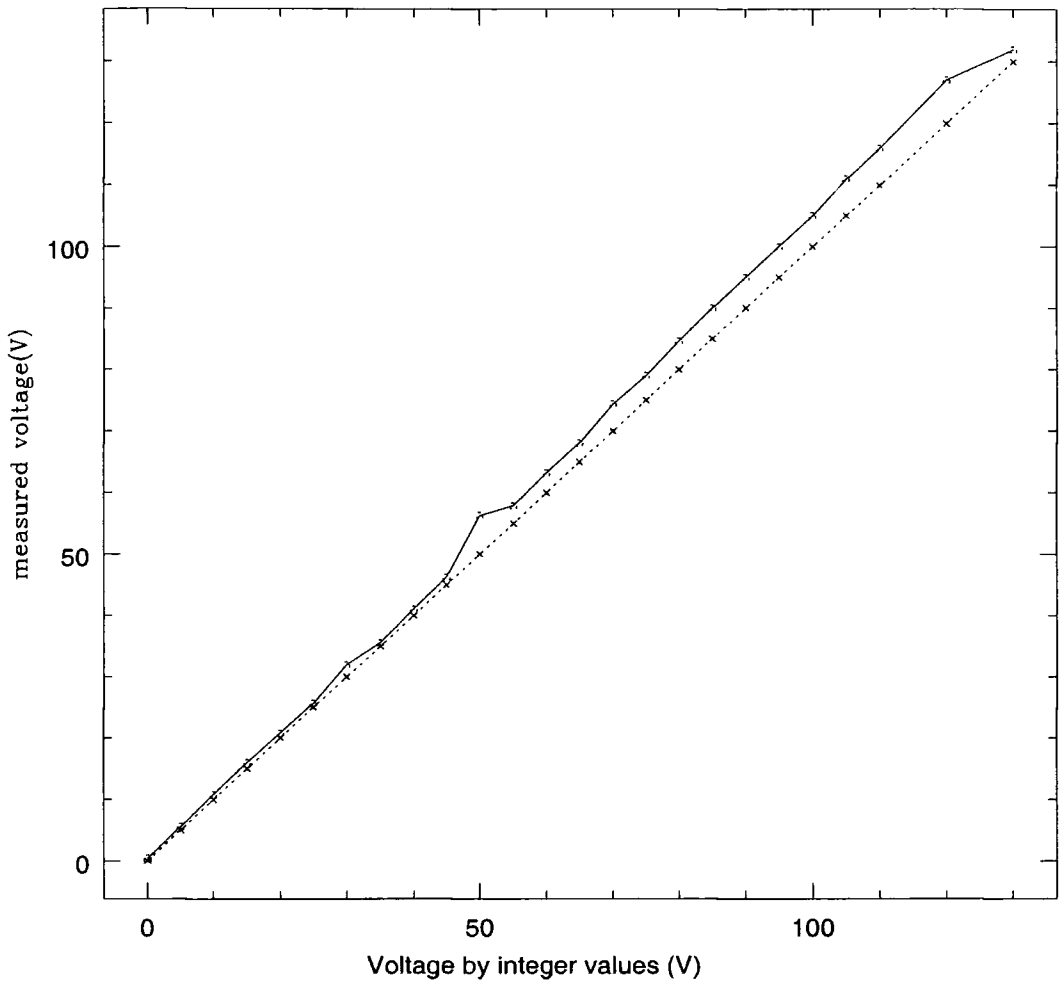

Figure 5.13: Calibration of the power supplies ouput. The integer values are entered in the PC using **mytest8.c**. The voltage is measured at the amplifier board ouput. The variations in the voltage were not taken into account because the important results are situated in the range of 50-130V where the voltage shift is quasi constant.

5.5 Atmospheric turbulence

The following section introduces the basis of the theory of atmospheric turbulence. For more detailed information, some references can be found at the end of this report [10][11].

5.5.1 Atmospheric turbulence

A major technical issue reducing the distortions of an image at the focus of a telescope is to remove the aberrations due to the turbulent layers which the light goes through before striking the primary mirror. The atmosphere acts like a set of small prisms with different indexes of refraction due to the random distribution of the temperature at a function of height. The result is a broadening and blurring of images far away from the diffraction limit.

5.5.2 Statistical model of the atmosphere and Fried parameter

Structure of atmospheric turbulence

The statistics of weak turbulence were introduced by Kolmogorov. He developed a model of the atmosphere based upon the fact that the refractive index at a given height fluctuates due to variations of temperature. The atmosphere is mainly detailed in two scales: the *outer scale* L_0 (typically in the order of a few hundred metres), where the main exchange of energy is due to wind shears, convections, and differential heating by the sun; and the *inner scale* l_0, a few cm, where the atmosphere dissipates its energy through molecular friction. The main assumptions of Kolmogorov were that the velocities and volume sizes can be described in a middle range (between L_0 and l_0, so typically of the order of the diameter of a telescope) where turbulence is isotropic (no prefered directions) and homogeneous (no variations between two different points). Beland[10] developed the general statistics of the theory of fluid mechanics. He introduced a function that correlates two independent points within the same volume: *the structure function* which can be written:

$$D(x\prime) = 2[C(0) - C(x\prime)]$$

where $C(0)$ is the variance defined from a statistical point of view as σ^2, the variance of the function, x is the relative distance to the center of the shell considered and $C(x\prime)$ is the autocorrelation function. The autocorrelation function is prefered as it relates absolute values without the need of a reference. The reference is taken at a random position within the volume.

One can calculate the power spectrum of a wide-sense stationary process just by Fourier transforming the autocorrelation function

$$\Phi(\kappa) = \int_{-\infty}^{+\infty} C(x\prime)exp(-2\pi i\kappa x\prime)dx$$

Kolmogorov argued that, in the inertial subrange defined by the two limits L_0 and l_0, the structure function is only dependent on ϵ, the coefficient of energy dissipation, of ν the coefficient of viscosity and the actual parameter r

$$D_v(r) = D(\epsilon, \nu, r)$$

Looking for the only combinations of ϵ and ν leading to a length and velocity dimensions variables, one finds the theoretical result of Tatarskii

$$D_v(r) = C_v^2 \epsilon^{2/3} r^{2/3}$$

where C_v^2 is the velocity structure constant and is a function of the altitude. Although the flow velocities do not interfere with the transmissions of light waves, the velocity structure function is a good starting point to the development of the interfering process description.

A more important feature is that the temperatures throughout the atmosphere are not constant. This variable can be considered a "conservative passive additive"[11] and then it can be shown that a similar power law describes the phenomenon and therefore a temperature structure function as follows

$$D_T(r) = C_T^2 r^{2/3}$$

where C_T^2 is the temperature structure constant.

Assuming that refractive index is a function of the density (thus proportional to $\frac{1}{T}$), the incoming light waves will be distorted. The refractive index structure is then

$$D(r) = C_n^2 r^{2/3}$$

It is easy to show that the temperature structure constant and the refractive structure constant are linked by the relation

$$C_n^2 = -80\times10^{-6}\frac{P}{T^2}C_T^2 \tag{5.1}$$

We can see that the refractive index fluctuations come about in a very specific way that is they are statistically defined by the value of this constant C_n^2, the strength of the turbulence. Using temperature sensors it is possible to calculate C_T^2 and then C_n^2. There are entire projects dedicated to determining the value of this coefficient. The description and understanding of the constant led to the understanding of the dynamic of the atmosphere. Models, such as Hufnagel[12], have been proposed and give a close approximate view of the reality.

Fried parameter and phase variations

Actual physical variations of a light beam in amplitude are less or even impossible to correct with an adaptive optics system. It appears important and more sensible to introduce another complementary definition of these electromagnetic waves: *the wavefront*. A wavefront is a surface which joins points of equal phase. When the light encounters the atmosphere, the plane wavefront coming from the source object is distorted. Shifts are introduced in the phase and the wave cannot be focussed into a diffraction-limited image. The phase fluctuation $\Phi(\vec{r})$ ($\vec{r}$ is a two-dimensional vector in the pupil plane), or wavefront aberration $(\lambda/2\pi)\Phi(\vec{r})$, is the quantity that is important. By definition, the complex amplitude of the incoming distorted wave of a given λ is then

$$U(\vec{r}) = U_0(\vec{r})exp(i\Phi\vec{r})$$

where $U_0(\vec{r})$ is the complex amplitude of the plane wavefront.
In the case of Kolmogorov turbulence, it can be shown that the covariance of the complex amplitude is given by

$$C(\vec{r}) = exp(-\frac{1}{2}D_\Phi(\vec{r}))$$

where $D_\Phi(\vec{r})$ is the *phase structure function* introduced earlier. For an infinite plane wave source placed at a distance R from the aperture plane (telescope for example) and assuming that the amplitude variations are small, the phase structure function becomes

$$D_\Phi(\vec{r}) = 2.91r^{\frac{5}{3}}k^2\int_0^R C_n^2 dz$$

k is the wave number and z the altitude of the turbulent layer. It is to be noted that the phase structure function $D_\Phi(\vec{r})$ is function of the turbulence strength C_n^2 so that the knowledge of this constant is enough to understand the structure of the atmosphere for different altitudes, and thus the turbulence to correct.

We now have to introduce a factor called the Fried parameter r_0 which defines the maximum length of an independant and correlated volume within the atmosphere[13]. It is defined as

$$D_\Phi(\vec{r}) = 6.88(\frac{r}{r_0})^{\frac{5}{3}}$$

then

$$r_0 \propto (k^{-2}\int_0^\infty C_n^2 dz)^{-\frac{3}{5}}$$

It can be seen that $r_0 \propto \lambda^{\frac{6}{5}}$. This parameter is important because it defines the real image quality at a certain wavelength taking into account the conditions of the observations. We recall that the diffraction limit is defined by $\alpha \propto (\lambda/D)$ where λ is the wavelength and D is the diameter of the primary mirror of the telescope. But in reality, the image quality is limited by the Fried parameter r_0 by $\alpha \propto (\lambda/r_0)$. r_0 can vary from a few cm to a meter in the best cases. We then see the bigger the value for r_0 the closer the image resolution will be to the diffraction limit. As the resolution is proportional to λ/r_0, it is wavelength dependent enough to be considered.

$\lambda = 0.55\mu m$	$\lambda = 1.2\mu m$	$\lambda = 1.6\mu m$	$\lambda = 2.2\mu m$
10	25	36	53
15	38	54	79
20	50	72	106

Table 5.2: Values of Fried parameter r_0 in cm at different wavelengths.

Table 5.2 gives some example of value of r_0 at different wavelengths.

Strehl Ratio

The *Strehl Ratio* S is the ratio of the central intensities of the aberrated PSF to the diffraction-limited PSF. It is directly related to the *variance* of the phase ${\sigma_\Phi}^2$ by the Gaussian function

$S \sim exp(-\sigma_\Phi^2)$. In the case of small aberrations, such as the random process of atmospheric turbulence, the Strehl becomes $S = 1 - \sigma_\Phi^2$. The higher S the better. However, a physical upper value limits the correction of the wavefront aberration: the Marechal criterion. It sets the value of S to 0.8 which is far enough and very difficult to reach in practice.

Zernicke Modes and applications to the Kolmogorov Turbulence

Wavefront errors induced by the turbulences can be decomposed into a set of orthogonal functions called the Zernicke polynomials. They are circular functions which can be used to represent a phase distribution over a telescope aperture in a mathematical form. It has to be noted that the Zernicke polynomials are not the only ones but they are the most commonly used for their ease and wide development. It was Noll[13] who first developed the applications of the Zernicke polynomials as we now know them:

for $m \neq 0$

$$Z_{evenj} = \sqrt{n+1} R_n^m(r) \sqrt{2} cosm\theta$$

$$Z_{oddj} = \sqrt{n+1} R_n^m(r) \sqrt{2} sinm\theta$$

or for m=0

$$Z_j = \sqrt{n+1} R_n^0(r)$$

where

$$R_n^m(r) = \sum_{s=0}^{(n-m)/2} \frac{(-1)^s (n-s)!}{s![(n+m)/2-s]![(n-m)/2-s]!} r^{n-2s}$$

where s is a mode index function of m (azimuthal frequency) and n (radial degree), both integers. Table 1.3 gives the value of these coefficients and their classical names.

The sixth column of Table 5.3 gives the value of the residual variance, or residual errors, $\Delta(rad^2)$ on the evaluation of the wavefront by means of the polynomials. 87% of the image aberrations can be removed just by correcting the low order modes specified above. For details about the development of the coefficients and their applications to the theory of the turbulent atmosphere see [11] and [13].

Z_j	n	m	expression	Aberration	residual variance $\Delta(rad^2)$
1	0	0	1	piston	$1.030(D/r_0)^{5/3}$
2	1	1	$2rcos\theta$	tilt	$0.582(D/r_0)^{5/3}$
3	1	1	$2rsin\theta$	tilt	$0.134(D/r_0)^{5/3}$
4	2	0	$\sqrt{3}2r^2-1$	defocus	$0.111(D/r_0)^{5/3}$
5	2	2	$\sqrt{6}r^2sin2\theta$	astigmatism	$0.0880(D/r_0)^{5/3}$
6	2	2	$\sqrt{6}r^2cos2\theta$	astigmatism	$0.0648(D/r_0)^{5/3}$
7	3	1	$\sqrt{8}(3r^3-2r)sin\theta$	coma	$0.0587(D/r_0)^{5/3}$
8	3	1	$\sqrt{8}(3r^3-2r)cos\theta$	coma	$0.0525(D/r_0)^{5/3}$
9	3	3	$\sqrt{8}r^3cos3\theta$	trefoil	$0.0463(D/r_0)^{5/3}$
10	3	3	$\sqrt{8}r^3sin3\theta$	trefoil	$0.0401(D/r_0)^{5/3}$
11	4	0	$\sqrt{5}(6r^4-6r^2+1)$	spherical	$0.0377(D/r_0)^{5/3}$

Table 5.3: Values of Fried parameter r_0 in cm at different wavelengths.

Bibliography

[1] G.V.VDOVINE, *Adaptive mirror micromachined in silicon* , Thesis, 1995

[2] B.C.BIGELOW *Deformable secondary mirrors for A.O* , Thesis, 1996

[3] C.R.KITCHIN *Astrophysical Techniques (second edition,1991)* , ISBN 0-7503-0137-6

[4] OKO Technologies, Delft University, Holland, *37-Channel micromachined AOS: Technical passport*, 1996

[5] G.VDOVINE, S.MIDDELHOEK, M.BARTEK, *Technology, characterization and applications of adaptive mirrors fabricated with IC-compatible micromachining*, SPIE, **2534**, 116-129

[6] S.TIMOCHENKO, *Theory of plates and shells*, McGraw-Hill, 1959

[7] A.S.SAADA, *Elasticity, Theory and applications*, Pergamon Press, 1974, ISBN 0-08-017053-6, Chapter 10

[8] W.H.BOWES, L.T.RUSSEL, G.T.SUTER, *Mechanics of Engineering materials*, John Wiley and Sons, 1984, ISBN 0-571-81070-3, Chapters 7-8

[9] E.KREYSZIG, *Advanced engineering mathematics*, John Wiley and Sons, Seventh edition 1993, p664-680

[10] R.R.BELAND, *Propagation through atmospheric turbulence*, Chap2 of **Infrared and Electro-Optic Systems Handbook**, Vol 2, Fred G.Smith, Ed., Spie Press and ERIM, 1993.

[11] V.I.TATARSKI, *The effects of the turbulent atmosphere on a wave propagation*, Israel Program for Scientific Translations (IPST), Jerusalem, 1971.

[12] R.E.HUFNAGEL, *Digest of Technical Paper, Topical meeting on Optical Propagation through Turbulence*, 1974.

[13] R.J.NOLL, *Zernicke Polynomials and Atmospheric Turbulence*, Journal of Opt. Society Am., **66 No3**, 1976.

[14] D.R.LIDE, *Handbook of Chemistry and Physics, 76th edition*, 1995-1996.

[15] Zygo Corporation, *ZyMod Phase Shifting System*, Operations Manual, 1992.

[16] Space Telescope Science Institute, *The Next Generation Space Telescope*, June 1997.

[17] G.G.HASELDEN, *Cryogenic Fundamentals*, Academic Press, 1971.

[18] F.DIN, A.H.COCKETT, *Low-Temperature Techniques*, Newnes.

[19] D.P.GREENWOOD, *Bandwidth Specification for Adaptive Optics Systems*, JOSA, **67**, 3, 1997.

[20] J.W. RAYLEIGH, *The theory of sound*, Dover, 1945.

[21] G.V.VDOVINE, S.MIDDELHOEK, M.BARTEK, M.BARTEK, P.M.SARRO, D.SOLOMATINE, *Characterisation and Applications of adaptive mirrors fabricated with IC-compatible micromachining*, Proceeding SPIE **2534** "Adaptive optical systems and applications", 116-129, 1995.

[22] R.K.TYSON, *Principles of adaptive optics*, Academic Press Inc, 1991.

[23] P.WANG, *Numerical and Matrix Methods in Structural Mechanics*, Wiley, 1966.